AFRL-RV-HA-TR-2007-1099

Turbulence Instrumentation for Stratospheric Airships

Mark L. Duell
Lawrence M. Saupe
Brent E. Barbeau
Kris D. Robinson
George Y. Jumper

September 2007

FINAL REPORT

AIR FORCE RESEARCH LABORATORY
Space Vehicles Directorate
29 Randolph Rd
AIR FORCE MATERIEL COMMAND
HANSCOM AIR FORCE BASE, MA 01731

AFRL-VS-HA-TR-2007-1099

This technical report has been reviewed and is approved for publication.

/signed/
Robert A. Morris, Chief
Battlespace Environment Division

/signed/
George Y. Jumper, Manager
Optical Turbulence Impact Program

/signed/
Paul Tracy, Acting Chief
Battlespace Surveillance Innovation Center

REPORT DOCUMENTATION PAGE

Form Approved
OMB No. 0704-0188

1. REPORT DATE *(DD-MM-YYYY)*	**2. REPORT TYPE**	**3. DATES COVERED** *(From - To)*
04-09-2007	FINAL	1 May 2006 – 04 Aug 2006

4. TITLE AND SUBTITLE
Turbulence Instrumentation for Stratospheric Airships

5a. CONTRACT NUMBER

5b. GRANT NUMBER

5c. PROGRAM ELEMENT NUMBER

6. AUTHOR(S)

Mark L. Duell, Lawrence M. Saupe, Brent E. Barbeau, Kris D. Robinson and George Y. Jumper

5d. PROJECT NUMBER
1010

5e. TASK NUMBER
0T

5f. WORK UNIT NUMBER
10100TA1

7. PERFORMING ORGANIZATION NAME(S) AND ADDRESS(ES)

Air Force Research Laboratory (AFRL)
AFRL/RVBYA
29 Randolph Road
Hanscom AFB, MA 01731-3010

8. PERFORMING ORGANIZATION REPORT NUMBER
AFRL-RV-HA-TR-2007-1099

9. SPONSORING / MONITORING AGENCY NAME(S) AND ADDRESS(ES)

10. SPONSOR/MONITOR'S ACRONYM(S)

11. SPONSOR/MONITOR'S REPORT NUMBER(S)

12. DISTRIBUTION / AVAILABILITY STATEMENT
APPROVED FOR PUBLIC RELEASE; DISTRIBUTION UNLIMITED

13. SUPPLEMENTARY NOTES

14. ABSTRACT

Both commercial and high altitude aircraft such as the U-2 may encounter turbulence in flight. The turbulence seems to be associated with buoyancy waves generated by flow over mountains that can break into turbulence. The exact nature of the wave breaking is not fully understood, and forecast models need to be examined to determine their ability to forecast turbulence. The High Altitude Airship is designed to investigate these phenomena. In order to sense atmospheric turbulence at altitudes of the expected flight of the High Altitude Airship of around 65,000ft, a prototype ionic anemometer was constructed. The instrument was checked out in flow at one atmosphere using an available flow channel. It was then checked in a Bell Jar at the density conditions expected at high altitude. For the remaining flow test at high altitudes, it was decided to construct an inexpensive wind tunnel which could operate under vacuum at near target altitudes. This report documents the design and checkout of the tunnel, and contains recommendations for further work.

15. SUBJECT TERMS
Wind tunnel, High altitude, Low density

16. SECURITY CLASSIFICATION OF:			**17. LIMITATION OF ABSTRACT**	**18. NUMBER OF PAGES**	**19a. NAME OF RESPONSIBLE PERSON**
a. REPORT	**b. ABSTRACT**	**c. THIS PAGE**			George Jumper
UNCL	UNCL	UNCL	UNL	50	**19b. TELEPHONE NUMBER** *(include area code)*

Contents

Contents (cont.)

Illustrations

Illustrations (cont.)

Tables

Preface

Many people have contributed to the success of this project and I would like to note the contributions of the individual co-authors. The project itself is a testament to the value that shorter term personnel can add to a program. The first two authors were not full time employees of the AFRL.

- Mark Duell came to us in the summer of 2005 as a "Space Scholar" (the AFRL/VS summer student intern program) from Embry-Riddle Aeronautical University, between his junior and senior year. His job the first year was to assemble and test the ionic anemometer at one atmosphere and in a bell jar. He returned after his senior year to assemble the low density wind tunnel we used to test and to perform a velocity calibration at the desired altitude. He probably would have completed that if the laboratory machine shop had not been assigned to higher priority tasking. He is currently employed by General Electric Infrastructure, Aviation, Lynn, MA.
- Larry Saupe, Maj (S) USAFR, began performing his reserve duty with us in the spring of 2005. He was an employee of General Electric Global Research, Niskayuna, NY. Larry brought an impressive professional background in aeronautical and mechanical engineering and a lot of experience with problems associated with power generation, heat transfer, and fluid flow. In the two and a half years he has been with us, serving only 24 days per year, Larry has contributed immensely in the area of tunnel configuration, pump and fan selection, heat transfer analyses, tunnel operation, and error analysis.
- Brent Barbeau, Capt USAF, has been working on related parts of this project since his arrival in May, 2004. He originally participated in the selection process for the high altitude anemometer. Next he worked with Maj Saupe, and mentored Mark Duell through his two summers with the project. When Mark left, Brent worked with Larry to complete the tunnel, and he ran the final testing and documentation of the ionic anemometer.
- Kris Robinson is an Electrical Engineer and in-house contractor working for Utah State University. He has been a major contributor to the electrical aspects of the project, to name some of them: initial assembly of power supply components to the anemometer, testing it and the other candidate instruments, assembling the data acquisition system, and assisting in the data analysis. He worked together with Capt Barbeau running the final checkout experiments.

There were also many other people who contributed to the program. They include, Paul Tracy, AFRL/VSBY, Lab Manager and Section Chief; Will Thorn, AFRL/VSBX who lent us much of the equipment needed for this project, and who gave us lots of great advice; Jack Ignazio, AFRL/VSBXR, who supplied the bell jar vacuum assembly and assisted us in its use; Radian Belu, Electrical Engineer and AFOSR Summer Research Fellow, currently at the Desert Research Institute, NV, who assisted with many high voltage aspects of the problem; Emmett Bishop, Electrical Engineering Intern from Wentworth Technical Institute for circuit design; and John Redwood, machinist with the AFRL/VS machine shop, who made the ionic anemometer. Lts. Mike Walker and James Baird were active participants in the earliest phases of the program. We are also indebted to Dr. Arje Nachman, our AFOSR sponsor for this basic research project.

1. INTRODUCTION

Aircraft occasionally encounter turbulence in flight. There has been considerable effort to try to forecast the occurrence of this turbulence by NASA, the FAA, NOAA, and NCAR. Systems are in place and are being evaluated to determine the best ways to detect turbulence and warn pilots[1]. High altitude aircraft, such as the U-2 also encounter turbulence, which is often Clear Air Turbulence or CAT, not associated with any thunderstorms or other convective activity. Often the turbulence appears to be associated with flight over mountains. It appears that a major cause is the gravity or buoyancy waves generated by flow over the mountains, which grow in amplitude as they ascend, until they are either absorbed into the flow by a critical layer, or until they break into turbulence[2]. The exact nature of the wave breaking, and the identification of exactly what conditions are dangerous to aircraft are not fully understood.

Most turbulence forecast models are not set up to operate at these altitudes, well above commercial airline flight. It is not certain that operating the models at the higher altitude would in fact capture these events, due to resolution at the high altitudes and other numerical problems. There are only a small number of forecast tools available to the high altitude pilot. One is the Mountain Wave Forecast Model (MWFM) operated by the Naval Research Laboratory[3], which uses ray tracing methods to project mountain waves through global forecast models. Other candidate forecast models will be examined to determine their ability to detect CAT conditions at high altitudes. There is always a problem of validating the output of any turbulence model (see Ref. 1). Ideally the output of the model should be compared to actual data, but when turbulence is forecast, no one wants to fly through it.

Recently[4], it was proposed that the US should investigate the utility of operating a blimp-like object at altitudes above 60 000 ft. This idea developed into the High Altitude Airship (HAA), an Advanced Concept Technology Demonstration project managed by the U.S. Army, funded through the Missile Defense Agency. Originally slated to fly in 2006, it has encountered some development problems, and is currently scheduled to fly in 2008. The HAA concept is to ferry itself from a home base to an operating location, then maintain station keeping for long periods of time. In studies of wind climatology at the target, it has been estimated that the airship should be able to sustained headwinds up to 30 knots. While considering the problems associated with the validation of high altitude CAT forecasts and the general lack of long term observations at high altitude, the HAA appears to be an ideal platform to study waves and turbulence at high altitudes. Not only would this help in the verification of wave and turbulence forecast models, but it would also provide the environmental specification for future stratospheric airship payloads

2. REQUIREMENTS

The design condition will be for a standard atmosphere at 60 000 ft (18 288 m): T=390 R (217 K), P=1.05 psi (7,230 Pa), ρ=0.000226 slugs/ft^3 (0.116 kg/m^3). The mean speed of the HAA based on climatology requires a sustained cruise speed of 30

knots[5] or 50 ft/s (15 m/s). The desired minimum wind variance is 3ft/s (1m/s). Minimal temporal sensitivity would be to detect a flow disturbance down to an eddy size of 1 m at 30 m/s, or 0.033 s. This would require at least 60 Hz for two data points per eddy at the maximum cruise speed. The reference altitude is 60 000 ft.

3. ALTERNATIVES

Four alternatives were considered for use as a high altitude velocity turbulence sensor: the pitot-static tube, the hot wire anemometer, the propeller anemometer, and the ionic anemometer, which was used by French scientist, Jean Barat for many high altitude measurements. The suitability of each for the required mission is analyzed below.

3.1 Pitot - Static Tube

A pitot-static tube is a flow velocity meter which is capable of measuring fluid velocities as a localized point (as opposed to an averaged velocity across a larger section). The pitot-static tube senses pressure at two locations: one in front – ideally the stagnation point where the flow stops yielding the "stagnation" or "total" pressure, and one on the side – ideally at a spot where the pressure is indicative of "free stream" or "static" pressure. For lower speed flows, the important quantity is the difference in the two pressures, known as the "dynamic pressure", which is typically measured with a differential pressure transducer. The fluid velocity can be obtained from the difference in pressure or dynamic pressure using incompressible fluid theory. These probes are also used for high speed flows, where Mach Number can be deduced from the ratio of the measured pressures, and speed is determined from a speed of sound calculation that requires the air temperature.

A flow can be considered incompressible if its velocity is less than 30% of its sonic velocity. For such a fluid, the Bernoulli equation describes the relationship between the velocity and pressure along a streamline:

$$\frac{v^2}{2g} + z + \frac{p}{\rho g} = C \tag{1}$$

Evaluated at two different points along a streamline, the Bernoulli equation yields:

$$\frac{v_1^2}{2g} + z_1 + \frac{p_1}{\rho g} = \frac{v_2^2}{2g} + z_2 + \frac{p_2}{\rho g} \tag{2}$$

If $z_1 = z_2$ and point 2 is a stagnation point, i.e., $v_2 = 0$, the above equation reduces to:

$$\frac{v_1^2}{2} + \frac{p_1}{\rho} = \frac{p_2}{\rho} \tag{3}$$

For instrument sensitivity, we compute the pressure difference for a 3 ft/s (~1 m/s) variance with various mean wind speeds up to 50 ft/s (~15 m/s). Solving for the pressure difference:

$$\Delta p = \frac{1}{2}\rho\left(\bar{v} + v'\right)^2 \tag{4}$$

The results are plotted in Figure 1. For the maximum mean wind velocity, the difference in pressure is a bit over 0.002 psi (17Pa), which decreases as wind velocity decreases. While pressure differences of this low magnitude are measurable, they are below what is commonly available for operational – long endurance use.

3.2 Hot Wire Anemometer

Since the main purpose of the project is to measure turbulence, a common laboratory solution is the hot wire anemometer, which was briefly considered for this application. A hot wire does lose some performance as air density decreases and the heat transfer coefficient is reduced[6]. Use at HAA altitudes reduces the frequency response to about one half of the sea level response. The primary concern is the need for long endurance. Hot wires must be very thin, typically 1μm, to achieve the required frequency response for turbulence. The net result is a rather fragile instrument, that would probably not be suitable for long endurance. The corner frequency (the highest frequency of good data) of a hot wire for a range of atmospheric density ratios, up to 1 (sea level density), and for a range of wire diameters from 5 to 50 μm is shown in Figure 2. The approximate density at HAA altitude is the at the left side of the curve.

The primary cause of decreased frequency response is the increase in wire diameter. In order to meet the 60 Hz requirements, the wire must be no greater than 7.5 μm in diameter, which is very thin from an endurance standpoint.

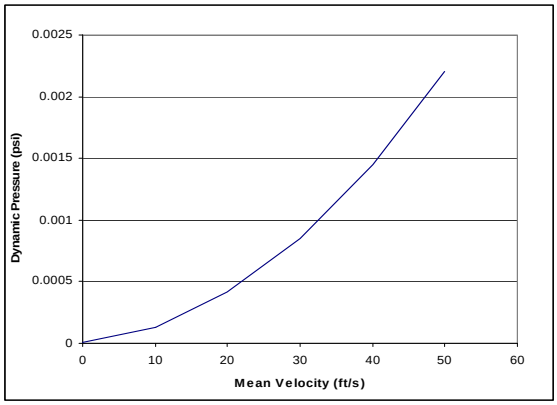

Figure 1. Pressure difference for a pitot-static probe at HAA altitudes for wind velocities up to 50ft/s for a velocity difference of 3ft/s.

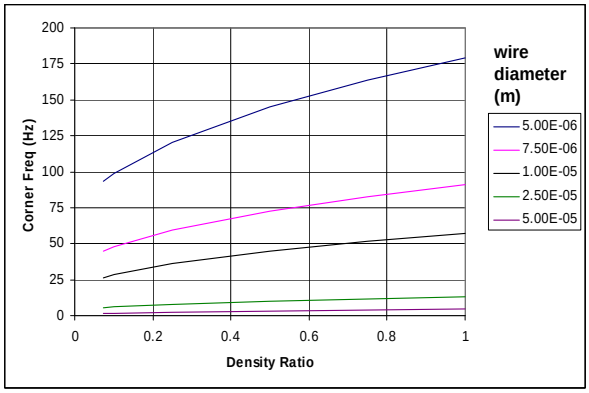

Figure 2. Corner frequency of a hot wire anemometer vs. atmospheric density ratio for various wire diameters

3.3 Propeller Anemometer

Anemometer devices have existed in various forms over the past several centuries. One of the more popular recent designs is the propeller anemometer, a device consisting of several propeller blades that rotate in the presence of an airflow. An example of one such device is depicted in Figure 3. The rate at which the propeller spins when encountering an airflow, is used to quantify the magnitude of that airflow.

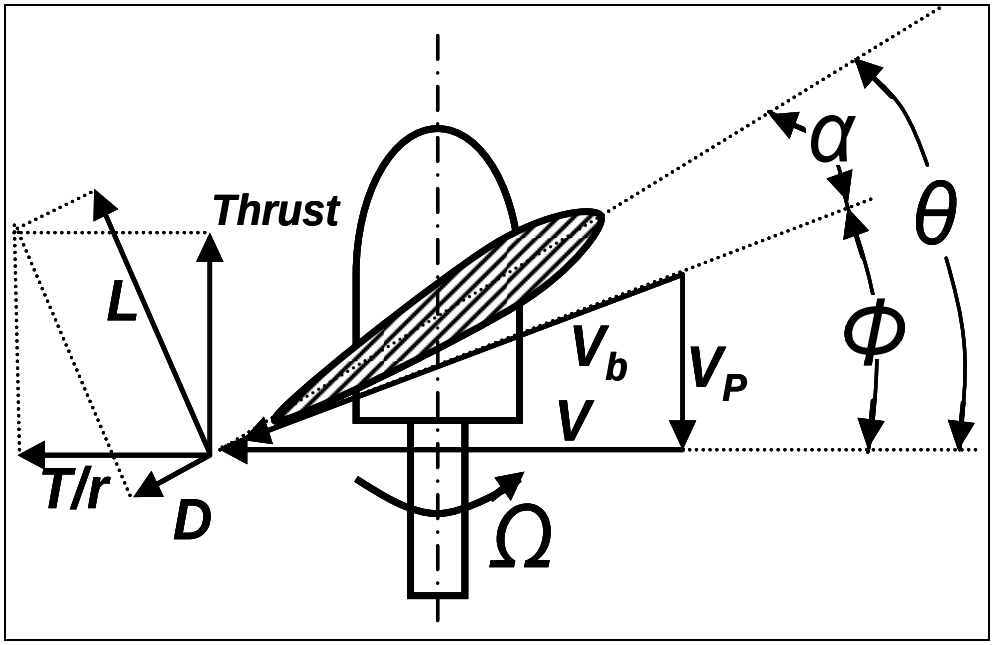

Figure 3. Cross sectional view of a propeller through one of the blades at a located a distance *r* from the axis of rotation. Lift, *L*, and drag, *D*, are referenced to the zero lift line. If the propeller is spinning at just the right speed to cause no thrust or drag on the propeller shaft, then all the airflow will be along the axis of the blade. V_p is the air velocity approaching the propeller, V is the rotational velocity approaching the blade, V_b is the total velocity flowing over the blade element.

3.3.1. Propeller Anemometer Theory

At moderate altitudes, a lightweight propeller anemometer with a high number of blades exhibiting a large surface area can measure airflows of small intensity, or small fluctuations in the mean airflow. The speed of the airflow is obtained by measuring the rate at which the airflow causes the propeller to rotate. A propeller anemometer is a logical candidate for the HAA; however the friction and inertia of the overall system, and the low air density at the desired altitude and low airspeed could make it an ineffective device on the HAA.

To predict the performance of a typical propeller anemometer on the HAA, a simulation of the propeller was examined using MATLAB®[7]. The model was run with the parameters of a commercial high quality turbulence sensing propeller anemometer made by the R.M. Young Company. Results of the simulations were compared to wind tunnel test results to fine-tune the model.

3.3.2. Propeller Anemometer Model

To derive a mathematical model for a propeller anemometer, we begin with the conservation of angular momentum equation, the rotational analog of Newton's 2nd Law:

$$\sum M = J\Omega' \tag{5}$$

where J is the total moment of inertia of the system, Ω' is the angular acceleration and ΣM is the sum of the moments on the propeller system, all about the axis of rotation.

An anemometer has three contributions to the inertia: propeller, shaft, and the motor. The moments on the anemometer are the torque from the propeller, *T*, and any rotational friction, expressed as a constant, b_T, multiplied by the rate of rotation:

$$(J_P + J_S + J_M)\Omega' = T - b_T\Omega \tag{6}$$

Since our main purpose is to see if an anemometer is even feasible at the altitude at which the HAA will fly, we first make some simplifying assumptions. If an ideal, frictionless anemometer does not give us the needed results, then it will not even be necessary to try computing one with all of the variables added. Therefore, we simplify the equation by ignoring damping and the inertias of the shaft and the motor, assumed to be much less than the propeller.

$$J_P\Omega' = T \tag{7}$$

Following blade element theory[8], for a thin section of the propeller blade at a distance r from the axis of rotation, the equation for incremental torque on a propeller is:

$$dT = r\left[\partial L \sin(\phi) + \partial D \cos(\phi)\right] \tag{8}$$

where ∂L is the incremental lift, and ∂D is the incremental drag, which will be ignored for this study. Lift is perpendicular to the zero lift line through the blade element, and ϕ is the angle between the lift vector and the thrust vector, which is also the difference between the local blade pitch angle (θ) and the angle of attack (α). Using the standard equation for lift in terms of a coefficient of lift, where V_b is the local flow velocity, C_L is the lift coefficient, *c* is the chord, *b* is the number of blades, and *dr* is the increment of radius:

$$dT = \frac{1}{2}\rho V_b^2 bc[C_L \sin(\phi)]rdr \tag{9}$$

Since C_L is assumed to be a linear function of α, it can be substituted using the following equation:

$$C_L = a(\theta - \phi) \tag{10}$$

In this equation, a represents the lift curve slope, assumed constant. The equation now becomes:

$$dT = \frac{1}{2}\rho V_b^2 bc[a(\theta - \phi)\sin(\phi)]rdr \tag{11}$$

As mentioned earlier, V_b is the section flow velocity, which is the vector sum of the axial flow into the propeller (V_p), and the angular flow velocity (V).

$$\bar{V}_b = \bar{V}_p + \bar{V} \tag{12}$$

The angular flow velocity is the product of the angular velocity of the blade and the radius at that point of the blade, $V = \Omega r$. The angle between Vp and V is ϕ. Using trigonometry we arrive at the following:

$$\tan(\phi) = \frac{V_p}{\Omega r} \qquad \sin(\phi) = \frac{V_p}{V_b}$$

Assuming ϕ is a small angle gives the following results: $\tan(\phi) = \phi$, $\phi = V_p / \Omega r$, and $V_b \approx V \approx \Omega r$. Note that this assumption can not be used when the blades have stopped or are rotating slowly relative to the wind speed. The Torque equation now becomes:

$$dT = \frac{1}{2}\rho\Omega^2 r^2 abc\left[\left(\theta - \frac{V_p}{\Omega r}\right)\frac{V_p}{\Omega r}\right]r\,dr \tag{13}$$

The equation for the pitch of an ideally twisted blade is: $\theta = \frac{\theta_t R}{r}$, where θ_t is the pitch angle at the blade tip, and R is the entire radius of the blade. Substituting for θ and multiplying the terms yields:

$$dT = (\frac{1}{2}\rho\Omega rabcV_p\theta_t R - \frac{1}{2}\rho rabcV_p^2)dr \tag{14}$$

The full propeller torque is the integral of the incremental torque from the inner radius, assumed to be zero to R, the full blade radius:

$$T = \tfrac{1}{2}\rho\Omega abcV_p\theta_t R\int_0^R rdr - \tfrac{1}{2}\rho abcV_p{}^2\int_0^R rdr \tag{15}$$

After the integration, and factoring the equation becomes:

$$T = \frac{1}{4}\rho abcV_p\theta_t R^3(\Omega - \frac{V_p}{\theta_t R}) \quad (16)$$

The differential equation for rotational velocity, Ω, is now:

$$J_p\Omega' - \frac{1}{4}\rho abcV_p\theta_t R^3(\Omega - \frac{V_p}{\theta_t R}) = 0 \quad (17)$$

This is a nonlinear differential equation. The term $V_p/\theta_t R$ is the rotational velocity that results in no thrust. The difference between actual rotation and the no thrust rotation is the "error" term that causes the blade rotational speed to increase or decrease. Also note that V_p and ρ are terms in the gain that are available to correct the speed error by changing the rotation rate of the propeller. MATLAB® was used to solve the equation.

3.3.3. Propeller Anemometer Tests:

In order to calibrate the model, the simulation was compared to actual results from a wind tunnel experiment. The anemometer used for the study was one leg of a triple propeller "Gill UVW Anemometer" sold by R.M. Young Company[9], Model 27005. The propeller is a four blade expanded polystyrene propeller, model 08274 EPS Propeller, made by the R.M. Young Company. The properties of this propeller were input as the variables in the MATLAB® model, and a simulation was run using the same initial conditions as the wind tunnel testing. These variables are shown below. The parameters of the blade are: R = 0.11m, c = 0.05m, mass = 0.011kg. The propeller inertia depends on the mass and radius of gyration of the propeller ($J_p=mR_g^2$). For the radius of gyration, we used 45% of the radius. The pitch angle was listed as 0.425rad in the catalog. The slope of the lift curves, *a*, is assumed to be 6.8/rad, a representative value for propellers. The test was run at approximately sea level conditions, with ρ = 1.2kg/m^3, with a wind speed of 7.6m/s. For these conditions, the pitch angle had to be adjusted to 0.51 radians to achieve the correct final speed.

A comparison of the wind tunnel data to the model is shown in Figure 4. The results, using the above variables shown as the blue dashes, labeled "Model 1" are somewhat disappointing. In talking to the manufacture, we found that some of our original assumptions were quite optimistic. For one thing, the combined moment of inertia is apparently more than what was used. Also, the company cites a non-negligible friction when the propeller is stopped. The company cites a sensitivity, or distance constant. as 1.0 m; which is an indication of the time to get to 63% of full velocity compared to the time it takes for 1 m of fluid to pass the blade. At this velocity, the time should have been 0.13 s. The moment of inertia for the blade was increased to achieve this result, which is also shown on the plot as Model 2. This is still about twice as fast as the actual data, but since we should have started at something other than zero speed, and since we had an older anemometer, we decided to use the company provided sensitivity.

Next the simulation was run for the design altitude, by changing the density. The simulation was run for a 1m/s step increase in wind-speed starting from 0, 10, 20, and 30 m/s. The times to the 63% point for sensitivity calculations were 10 s, 1 s, 0.45 s, and

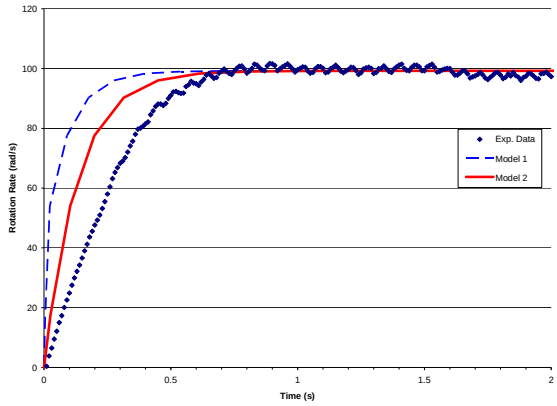

Figure 4. Propeller rotation rate vs time. Comparison of simulations to wind tunnel data. Wind tunnel data is represented by the dots, Original model is dashed. The solid curve uses manufacturers sensitivity.

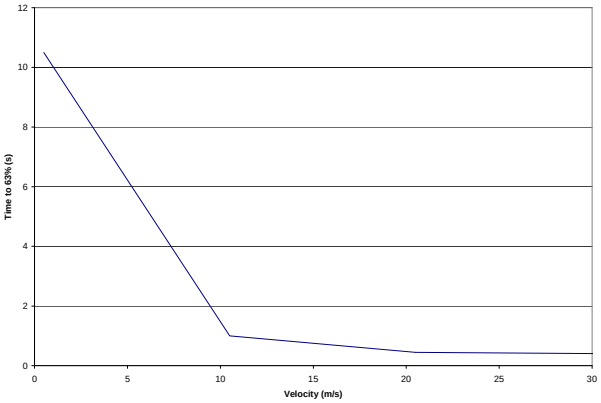

Figure 5. Estimated time to reach 63% of steady state vs. wind speed (velocity) at 65 000 ft altitude, using the manufacturer's sensitivity in the simulation.

0.4 s respectively, shown in the plot in Figure 5. This equates to a distance constant of around 10 m, an order of magnitude higher than the sea level value quoted by the manufacturer. Clearly the low density takes a toll on the responsiveness of the system, and would prohibit the instrument from meeting the desired response rate of the velocity turbulence sensor. The use of propellers, shafts, and sensors with lower moments of inertia is possible, but this action would impact instrument durability and serviceability.

3.4. Ionic Anemometer

A one dimensional ionic anemometer, that is, capable of measuring only one velocity component, consists of three parallel wires: one emitter wire and two collector wires on opposite sides of the emitter at equal distance. When a large potential difference (voltage) is applied between the emitter and collector, some air particles near the emitter are ionized (believed to be primarily $(H_2O)_nO_2^+$ and $(H_2O)_nN_2^+$). This voltage is the activation voltage; it is on the order of tens of kilovolts for a 1cm separation at 1 atmosphere. The electric field between the emitter and collectors accelerates the ions toward the collectors, producing a small current flow (on the order of microamperes). The acceleration of these ions occurs in negligible distance and they travel the majority of the distance at a steady state velocity, V_i, determined by the strength of the electric field, density of the air, and humidity of the air. One must insure that the voltage stays low enough to avoid arcing.

3.4.1 Ionic Anemometer Theory

In reported high altitude experiments, J. Barat[10] used two ionic anemometer designs to analyze the stratospheric winds; one used pulsed voltage to create ions, the second used continuous ionic flow. We focused on the latter. He found that the design operated well between 200 and 10 hPa (40 000 to 100 000 ft), had a detection limit better than 1 cm s^{-1}, an overall accuracy better than 10%, a response time constant lower than 10^{-2} s, and was

sufficient to measure CAT in the stratosphere. Barat gives the equation for ion velocity, V_i:

$$V_i = \mu^+ E \tag{18}$$

where μ^+ is the mobility of the ions and E is the strength of the electric field. The mobility μ^+ is a function of density:

$$\mu^+ = \mu_0^+ / \rho \tag{19}$$

where μ_0^+ is the reduced mobility, a function of humidity, but independent of dry air density, ρ. As the air density decreases, the mobility of the ions increases, and thus the required E field strength for a desired velocity decreases.

Consider the one dimensional anemometer in Figure 6 (designed to measure velocity in only one direction). Ions are released from the central emitter in all directions, with a slow initial velocity that rapidly comes up to the ion velocity relative to the air velocity. If the same number of positive ions went to the left as to the right, the ion density would be higher on the upstream side, which would locally modify the electric field. This must encourage more ions to drift downstream, tending to equalize the ion density. The density of the positive ions must be approximately constant within the instrument, since it has been found that for the collectors upstream (1) and downstream (2):

$$i_1 \propto V_i - V_\infty \text{ and } i_2 \propto V_i + V_\infty \tag{20}$$

Assuming the constants are the same (symmetrical instrument), this yields:

$$\Delta i \propto (V_i - V_\infty) - (V_i + V_\infty) = 2V_\infty \tag{21}$$

$$\Sigma i \propto (V_i - V_\infty) + (V_i + V_\infty) = 2V_i \tag{22}$$

Dividing Eq. (21) by Eq. (22) and rearranging yields:

$$V_\infty = K V_i \left(\Delta i / \Sigma i \right) \tag{23}$$

where K is the sensitivity constant. In normal use, V_i should be constant in the presence of changing wind conditions.

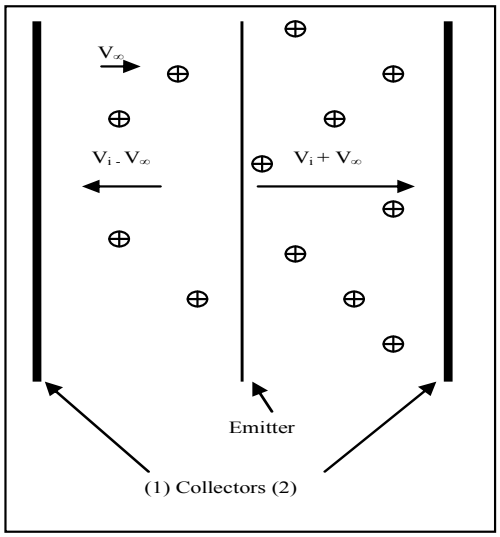

Figure 6. Schematic of a one dimensional ionic anemometer.

As a preliminary test we need to find the activation voltage and size of the region that is usable for measurements. For sensitivity calibration, we need to find the slopes (sensitivity constant) and intercepts (due to non-symmetry) of velocity vs. $\Delta i/\Sigma i$ curves for several voltages. For density calibration, we needed to find the activation voltage and verify operation in low density humid and dry air. The transit time for each of the ions

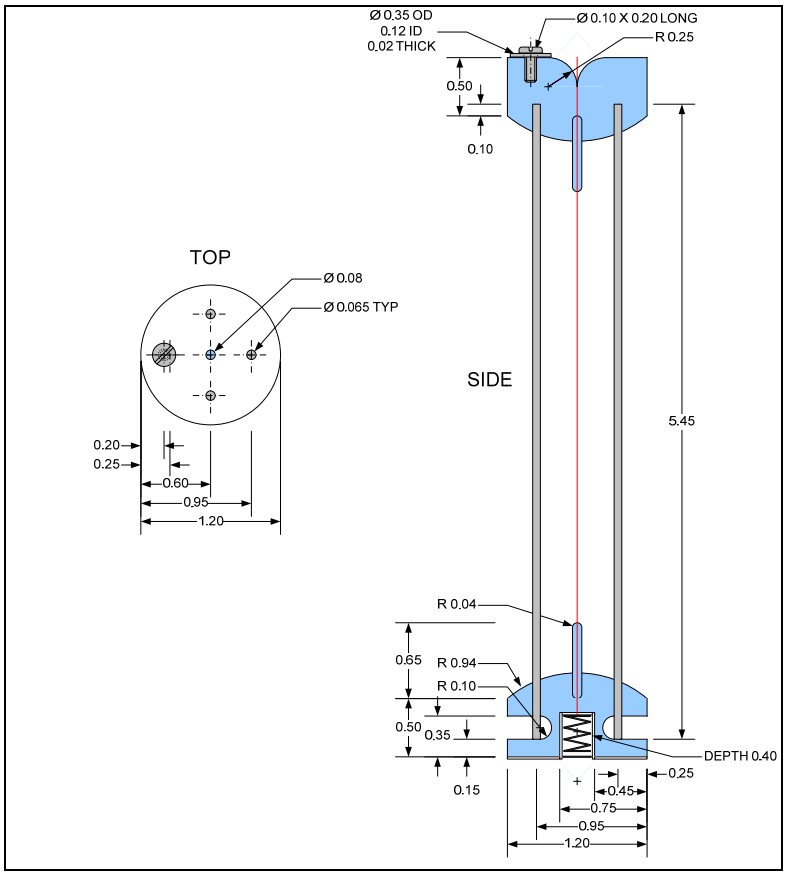

Figure 7. Top and cross-sectional view of the ionic anemometer. Units are in inches. Center electrode is tensioned by spring in the bottom housing and friction from the machine screw on the top housing.

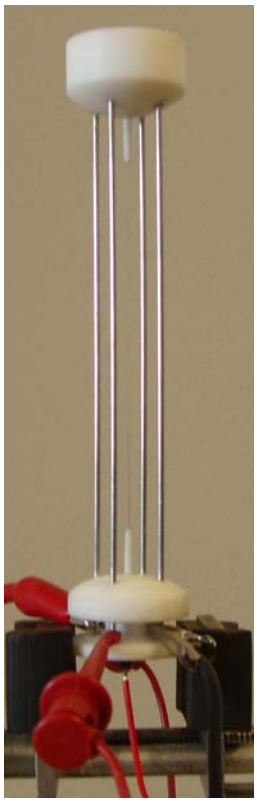

Figure 8. Photograph of the ionic anemometer attached to the high voltage leads and ammeters.

from emitter to collector is believed to be very short, giving the instrument a rapid response time to changing wind conditions allowing for the desired frequency of response (400Hz). The von Karman frequency of the flow passing over the collectors ranges from 6 Hz at 1 ft/sec to 2 kHz at 70 ft/sec and may cause fluctuations at some velocities in the desired usable range. Adding additional collectors (e.g. to determine velocity in the perpendicular plane) increases the strength of the electric field, which changes the ionic drift speed, activation voltage, and current.

3.4.2. Ionic Anemometer Hardware

The overall shape and design of the instrument, shown in Figures 7 and 8, were based on Barat's design. The overall length of the instrument is 0.15 m, with a diameter of 0.03

m. It is desirable to have a very fine emitter wire (20 – 120 μm is typical); 100 μm Tungsten was chosen for durability and availability. The collector rods are structural members, and thus must be sized to withstand anticipated loads; however large collectors create higher magnitude, lower frequency turbulence, so minimizing their size is desired. Aluminum rods 1.6 mm in diameter were selected for the collectors since they are expected to be sufficient and available. The overall length of the collectors is 0.14 m, with an exposed length of 0.12 m. The emitter wire has an exposed length of 0.09 m; there is some shielding at either end so that slightly off-axis winds do not affect total current readings. Both the emitter and collectors are free from any surface coatings or finishes in order to maximize electric conductivity. Some ionic anemometers use radioactive coatings on the emitter to aid in the production of ions. These coatings greatly reduce the voltage requirement (by approximately two orders of magnitude), but they also limit instrument life and add significant complexity to instrument construction, availability, and handling. We elected to use higher voltages instead of radioactive coatings, which present their own concerns. When dealing with high voltage (especially during the 1 atmosphere tests on the ground), suitable spacing of all parts, insulation, and connectors as well as proper safety procedures must be used. The structural disks at each end must be electrically insulating between the emitter and collectors. Teflon was selected for its durability, low temperature behavior, availability, and lack of outgassing at low pressures. Outgassing was also a concern in the choice of adhesives, and the outgassing from the superglue we selected was verified to be sufficiently low at expected flight pressures. The emitter wire is tensioned by means of a plate soldered to the end of it and a compressed spring in the base of the instrument. This forces the emitter wire to remain straight even when temperature changes cause the length of the collectors to change. At the top of the instrument the wire is held in place by friction between a screw and the Teflon disk. An electric connection is maintained by a thin copper shim that fits around the spring and provides a lead to the outside.

3.4.3. Ionic Anemometer Preliminary Testing

The anemometer was placed in a test stand with positive high voltage connected to the emitter and two collectors on opposite sides connected to separate micro ammeters. The two other collectors were connected to ground. To determine the activation voltage, the voltage was increased from zero until one of the ammeters read 0.2 μa. This voltage/current data were recorded. To determine the charge characteristic, shown in Figure 9, the voltage was further increased to 125% of the activation voltage and the voltage/current data were recorded at regular intervals. The voltage was then decreased until shut-off, recording the data at regular intervals.

For velocity calibration at sea level, the voltage was set to 105% of activation, and the currents were recorded at various wind speeds (including no wind). This was repeated at 110%, 115%, and 120% of activation voltage. The current difference divided by the sum was plotted versus velocity in Figure 10. At either of the two applied voltages, the response to velocity appears quite linear, indicating a constant sensitivity.

Next, the probe anemometer was tested at lower pressures, near those expected at operating altitude near 60 000 ft. The instrument was placed in a bell jar, and pressure

was drawn down to 73 hPa, approximately 7% of standard sea-level atmospheric pressure. First the single collector current was measured as a function of voltage, now much lower, as expected. The pressure in the jar was then drawn to near vacuum, then refilled to 73 hPa with dry nitrogen and the test was repeated. The results, shown in Figure 11, were similar to the sea-level curves, but at significantly lower voltages. While a calibrated flow source was not available in the bell jar, a computer cooling fan that could be run at two input voltages was placed near the anemometer. The current difference over the sum is shown for 4 applied voltages in Figure 12.

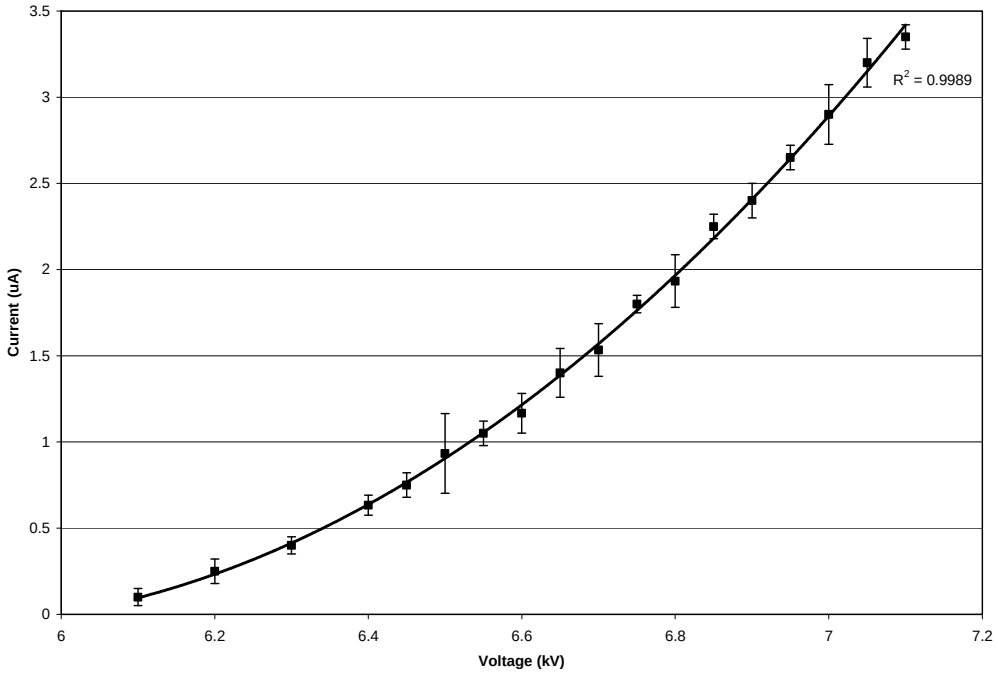

Figure 9. Current (μA) vs. applied voltage (kV) for a single collector at 1010 hPa.

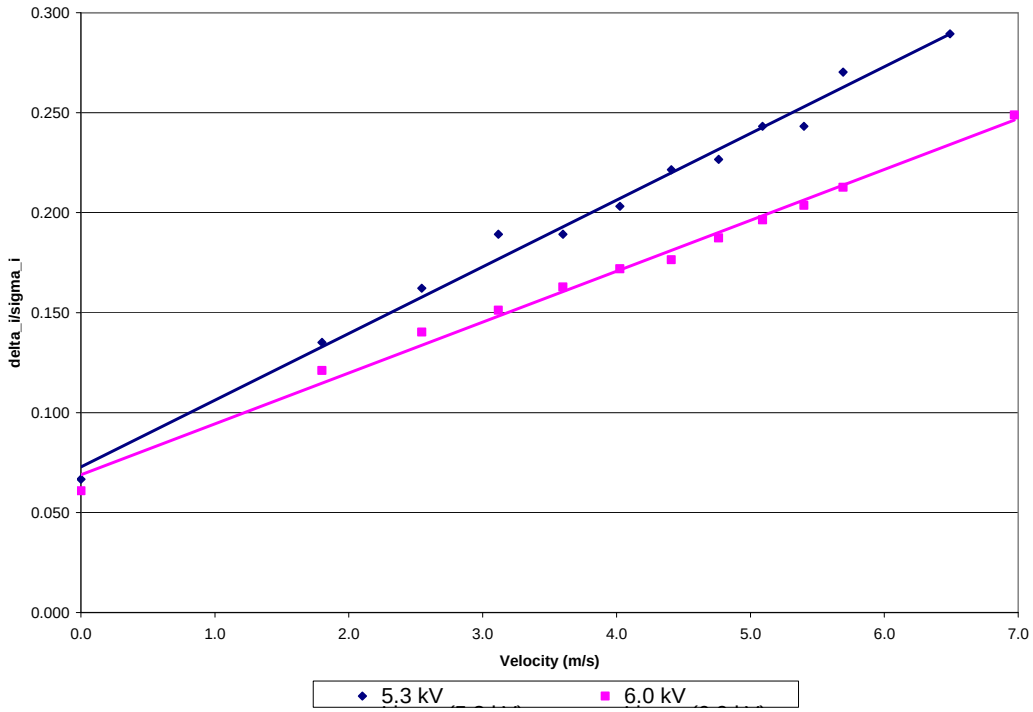

Figure 10. Velocity calibration for two collectors at 1010 hPa and two applied voltages, 5.3 and 6.0kV.

To determine the effect of density, the activation voltage was measured as described above, at densities from pressures at 60 000 ft down to those at around 20 000 ft. Those results are shown in Figure 13. The activation voltage increased from 1kV to 3kV as pressure increased, as expected.

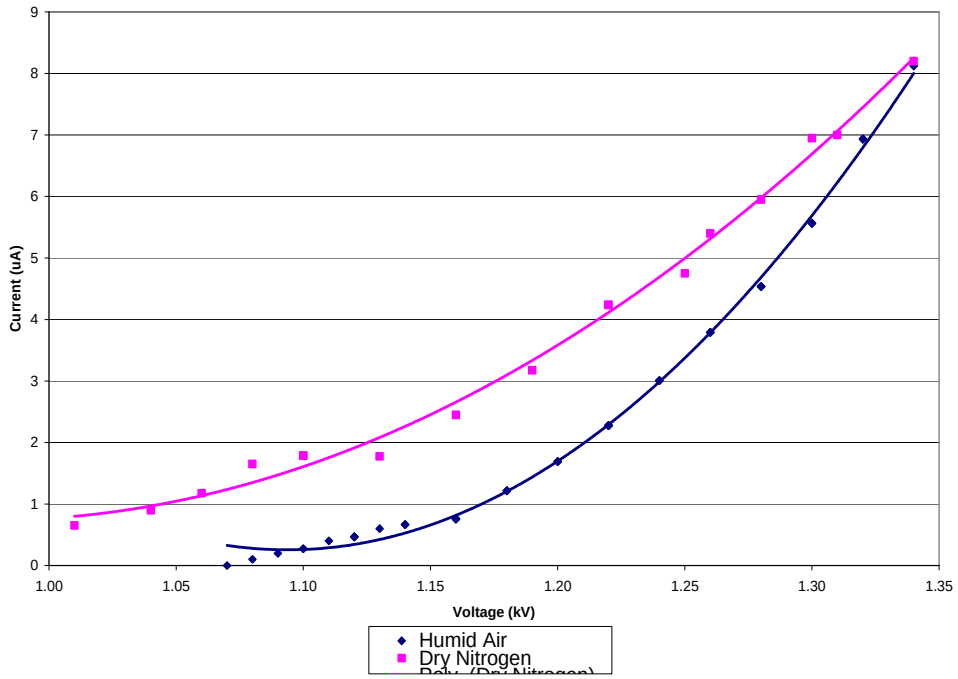

Figure 11. Current (μA) vs. applied voltage (kV) for two collectors in dry N_2 and humid air at 73 hPa.

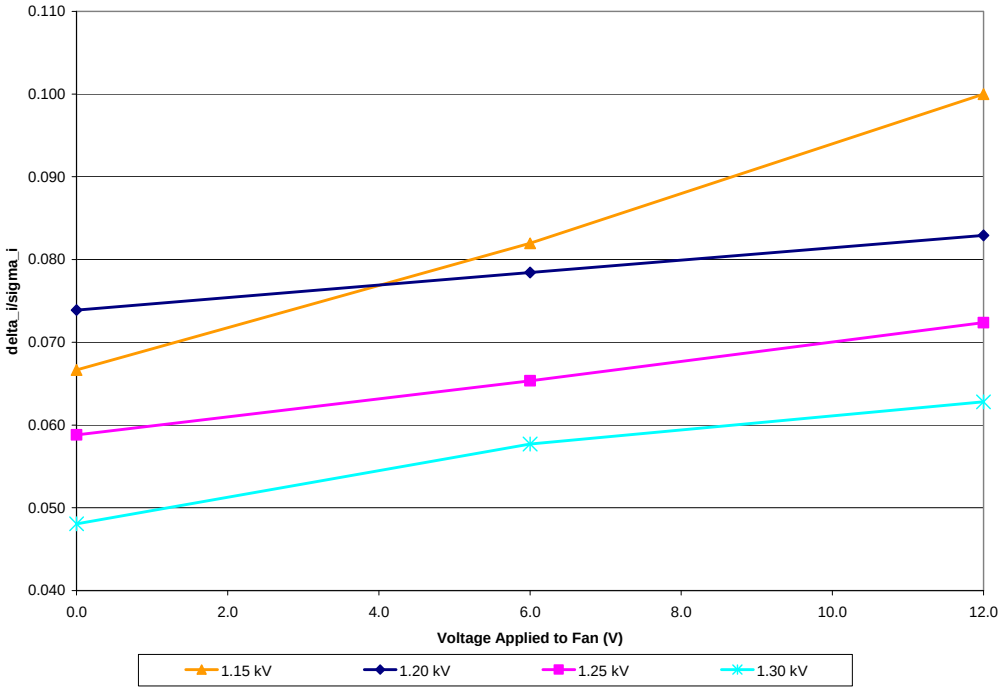

Figure 12. Velocity calibration for two collectors in dry N_2 at 73 hPa as shown at various applied voltages to the emitter.

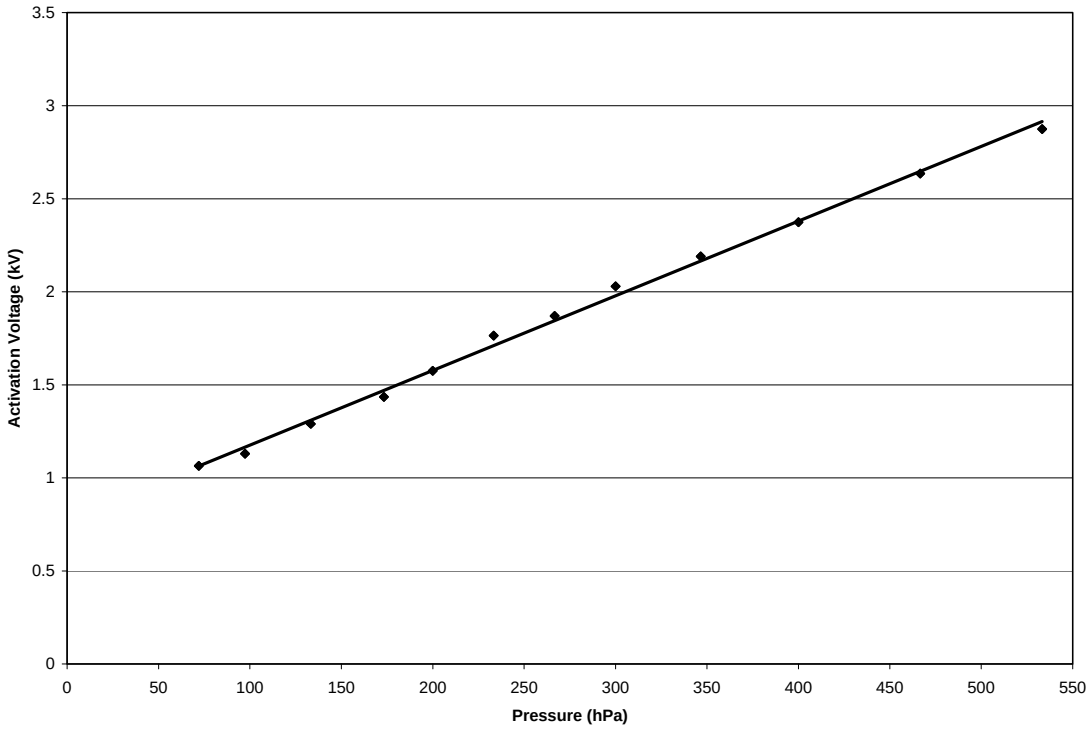

Figure 13. Density Calibration for Two Collectors in Dry N_2.

4. LOW DENSITY TUNNEL SELECTION PROCESS

4.1 Introduction

As part of the High Altitude Airship (HAA) payload program, a test cell is desired to replicate several in-flight atmospheric conditions that may be experienced by proposed test instrumentation during flight. This test cell would primarily be used to validate predicted instrument response to high altitude, low density conditions.

Key parameters for this test cell are duplication of the air density and velocity encountered in actual flight conditions. Air density is chosen to be that which would be experienced during S*tandard Atmosphere*[11] conditions at 60 000 ft. Chosen flight velocity is 30 knots (which has been assumed as 30 knots *true* airspeed). The test cell has been initially desired to have a circular cross section with an internal diameter of 8.0 inches.

Three different approaches are outlined in this report: *Once Through*, *Closed Loop Vacuum Pump* and *Closed Loop Fan*. Of the three, *Closed Loop Fan* appears to be initially most attractive due to its simple construction, ease of use, low initial cost and low cost of operation. However, depending upon equipment availability and duration of testing, other options may ultimately prove more desirable. The three configurations are shown in Figures 17, 18, and 19.

4.2 Test Cell Parameters

Table 1 outlines the actual and desired test conditions for this test cell (utilizing air as a test fluid).

Table 1. Actual and desired test cell conditions

Parameter	***Std Atm @ 60,000 ft***	***Test Cell w/Air***
Pressure (millibar) mmHgA	(72.312) 54.24	(98.22) 73.67
Temperature (^oC) ^oF	(-56.5) -69.7	(21.1) 70.0
Density (kg/m^3) lb/ft^3 *	(0.11628) 0.007262	(0.11628) 0.007262
Velocity (knots) ft/s	(30.0) 50.6	(30.0) 50.6
C (knots) ft/s	(573.8) 968.5	(668.7) 1128.7
Mach #	0.05228	0.04863
Vdot 8" dia duct (m^3/min) ft^3/min	(30.03) 1060.5	(30.03) 1060.5
Mdot 8" dia duct (kg/hr) lb/hr*	(209.6) 462.1	(209.6) 462.1
Dynamic ΔP head (cm-H_2O) in-H_2O	(0.1414) 0.05567	(0.1414) 0.05567
Reynolds Number (duct diameter)	25,652	20,051

* *Assumes G as 32.174 ft/s^2*

4.3 Once Through configuration

A *Once Through* configuration is initially proposed due to its inherent simple construction and a readily available high vacuum source (Busch vacuum pumps) at Hanscom AFRL.

A proposed flow schematic is provided in Figure 17. For this configuration, atmospheric air is drawn into the system through one or more critical flow nozzles. These flow nozzles will provide two important functions; 1) dramatically lower the stagnation pressure of the flow {due to the highly non-isentropic nature of the downstream shocks encountered} and 2) provide very accurate metering of the air flow (when critical, flow is only a function of atmospheric upstream pressure and temperature). Design standards for this type of vacuum "load chamber" configuration are available[12]. Major Saupe can provide design guidance as well.

Although readily calculable (as enthalpy is conserved for this type of flow), downstream stagnation temperature will be very near to that for upstream stagnation conditions (useful for first pass estimates).

Flow is brought off the end of the ASME style critical flow nozzle at a 90^{o} angle to the main flow direction. This is to further aid in breaking down the sonic (or possibly supersonic) flow and also aid in entropy production (further lower the stagnation pressure of the flow). One key operational note is that critical flow is assured when these flow nozzles become silent (as downstream sound waves cannot propagate upstream against sonic flow in the nozzle).

Vacuum pumps, whether liquid ring type, vane type or ejectors operate on a specific performance curve. Lowering the mass flow rate to the pump will typically result in lower absolute suction pressures. These pumps are essentially constant volume flow machines, though volume flow capacity can change over suction pressure ranges due to inefficiencies within the pumps (typically at low and high mass flow rates). OEM performance curves should always be consulted when using a vacuum pump to ensure performance will meet requirements over the range of flows and pressures anticipated (see generic vacuum system curve shown in Figure 14).

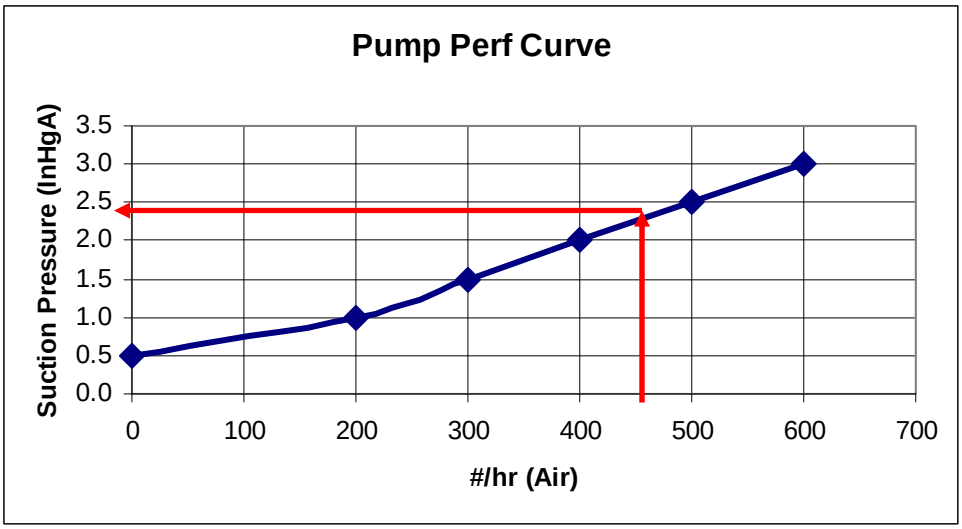

Figure 14. Generic vacuum pump performance curve. Typical industrial units are inches of mercury absolute (inHgA) for pressure and pounds per hour for flow rate (#/hr)

In the configuration provided in Figure 17, test cell pressure is provided by a valve positioned downstream of the test section. As the pump suction pressure is constant (the result of a constant mass flow rate fixed by the flow orifice), this valve will serve as a pressure drop device to adjust cell pressure at a desired level above pump suction pressure.

Although more complex, another approach would be to provide a recycle loop around the pump (or even a metered external air leak) such that the pump sees more inlet mass flow and will then ride up its performance curve to a new steady state higher pressure. Varying pump RPM is one option as well (though there may be practical limits to this approach).

Due to the very low dynamic head of this system, actual flow velocity measurements using traditional head change methods (such as pitot tubes, venturi tubes etc.) appear difficult. Knowing the mass flow rate (as provided by the flow nozzles) will enable velocity to be calculated, on an average sense, to a fairly high degree of accuracy. Local velocities could possibly be measured by other means such as hot wire probes or calibrated turbines. Mass flow rates in the system can also be cross checked against a flow meter placed at the vacuum pump discharge and/or by using the vacuum pump performance curve.

4.3.1 Minimum Vacuum Pump Requirements

For the prescribed flow conditions and geometry, the pump required will need to pump 1060 ACFM (Actual Cubic Feet per Minute) of air from 73.67 mmHgA (2.90 inHgA) to 760 mmHgA (29.92 inHgA) prior to accounting for line losses. Hanscom AFRL currently has a Bush vacuum pump that can handle 117 ACFM at 73.67 mmHgA (using a 7.5 HP electric motor). Initial estimates would require a pump similar to that

encountered in a municipal steam turbine power plant bottoming cycle, typically a liquid ring single or two stage pump, consuming close to 150 HP. Steam jet ejectors could be used as well, and would consume approximately 1700 lb/hr of motive steam and 150 GPM of cooling water[13].

If run times were to be short, the possibility of using a vacuum "accumulator" could also be investigated. A large vessel evacuated to a pressure much lower than 76 mmHgA could be initially evacuated over time to provide a short run of large capacity vacuum source.

Vacuum capacity requirements could be marginally reduced however by operating with the system at a higher air temperature (i.e. resulting in a higher pressure for a given density requirement), see Figure 15. A chiller placed just upstream of the pump could then serve to lower the ACFM entering the pump.

It is anticipated that due to the large costs associated with procuring and operating a vacuum system of this magnitude this configuration may not be desirable.

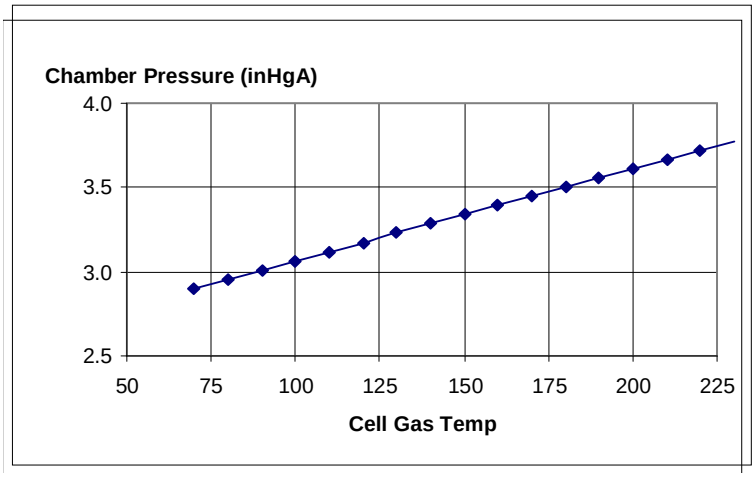

Figure 15. Required chamber pressure vs. test cell temperature (F)

4.4 Closed Loop Vacuum Pump configuration

The *Closed Loop Vacuum Pump* configuration is nearly identical to the *Once Through* configuration with the exception that instead of drawing from, and discharging to, open atmosphere, the working fluid is placed in a closed loop configuration utilizing the use of a retainment vessel (see Figure 18).

In this configuration it would be possible to change the working fluid to one with a much lower molecular weight (MW) than that of air. This change would result in a much higher absolute test cell pressure and smaller vacuum system ΔP requirements for the prescribed density. Figure 16 illustrates the effect on pump suction pressure of lowering MW.

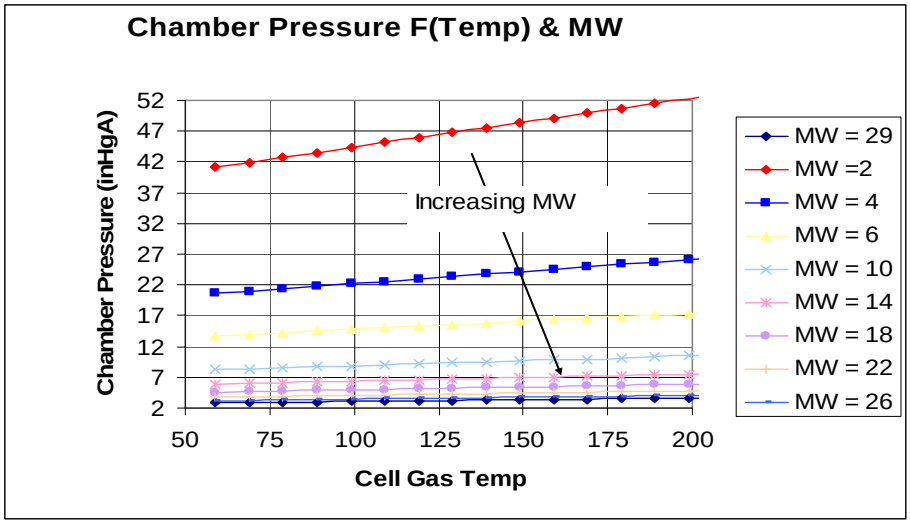

Figure 16. Effect of molecular weight and temperature (°F) on test cell operating pressure.

The plot indicates that as MW decreases, vacuum pump ΔP performance requirements are lowered, until for very low MW (such as with Hydrogen) chamber pressure could actually be higher than atmospheric. In such cases, a vacuum pump could be replaced by a much more economical centrifugal pump or blower for circulation. Obtaining and retaining gas purity in such a system may prove formidable however.

The same advantages remain in this system with regard to known flow rates via critical flow nozzles and pump performance curves. Instrumentation to be tested in the cell should be validated as suitable for whatever fluid is chosen.

4.5 Closed Loop Fan configuration

The *Closed Loop Fan* configuration is shown in Figure 19. In this configuration air is used as the test fluid and is circulated via a fan (similar to a closed loop wind tunnel). Air density is controlled through the use of an external vacuum pump. In this manner a vacuum pump is used to initially evacuate the test system down to a prescribed density. A fan then circulates the flow. The vacuum pump remains in standby mode to remove any air that should it leak into the system or counter any increase in gas temperature. The vacuum pump used for this application could be rather small (provided air in-leakage to the system was minimal).

This configuration has the advantage of low capital cost and low cost of operation. One disadvantage stems from determining an accurate method of flow measurement. The very low dynamic heads associated with this type of flow may require some sort of hot wire probing or low mass turbine insertion into the flow field.

Fan sizes and performance would need to be looked at closely in order to ensure adequate performance. Line losses should also be closely reviewed.

As a first estimate, a circulation fan capable of handling 1060 ACFM of air would typically have a blade diameter of 12". Capacity would be largely a function of backpressure (line loss). If the test section were to be constructed of four lengths of straight pipe and four elbows, line losses may be on the order of that shown in Table 2.

Flow Conditions:
- Air @ 462 #/hr, 70^{o} F and 74 mmHgA

Piping:
- Four elbows (L/D = 20)
- Two 10 foot sections of pipe
- Two 4 foot sections of pipe

Material:
- PVC piping and clear Lexan

Dimensions:
- 12", 10" or 8" I.D. Main Piping w/ 8" I.D. of flow test section

Table 2. Estimate of line losses[3]

Parameter	***12" Main Pipe***	***10" Main Pipe***	***8" Main Pipe***
Velocity in 12" Pipe (ft/s)	22.4	22.4	22.4
Velocity in 8" Test Section (ft/s)	50.6	50.6	50.6
ΔP per foot of main pipe (inH_2O)	0.00038	0.00091	0.00267
ΔP per total pipe 28 ft (inH_2O)	0.01088	0.02588	0.07506
ΔP per Elbow (inH_2O)	0.00776	0.01543	0.03574
ΔP per 4 Elbows (inH_2O)	0.03102	0.06167	0.14300
8" Test Section (est) (inH_2O)	0.02500	0.02500	0.02500
Total Estimated Pressure Drop (inH_2O)	*0.06689*	*0.11255*	*0.24306*

A typical 12" circulation fan, such as Dayton Fan's axial duct Model 4TM80 has the following performance at *standard atmosphere* sea level conditions:

1627 ACFM @ 0.000 inH_2O backpressure 1182 ACFM @ 0.250 inH_2O backpressure
1465 ACFM @ 0.125 inH_2O backpressure

As test density is far below that at standard atmosphere sea level conditions, various fan laws must be employed to estimate capabilities at these lower densities.

The following "test condition" performance for this fan is estimated using on-line conversion programs at http://www.torringtonresearch.com/fancalc.html

Table 3. Estimate of fan performance in low density conditions

Parameter	*Sea Level Density*	*Test Density*
Max allowable back pressure (inH_2O) at 1627 ACFM	0.00	0.00
Max allowable back pressure (inH_2O) at 1465 ACFM	0.125	0.010
Max allowable back pressure (inH_2O) at 1182 ACFM	0.250	0.020
Nominal HP	0.25	0.025
RPM	1750	1750

As shown on Table 3, it quickly becomes apparent that much care must be used when selecting a fan for this duty. In this case, a 12" fan may not be able to overcome the anticipated pressure drop in the system. Alternate fan designs, blowers or propellers designed for high altitudes may need to be employed in order to provide the needed flow rate at the estimated back pressure. Staging of axial fans could also be considered. Exceeding a fan's rated maximum discharge pressure should be avoided, as stalling of the blades could be one possible outcome. One useful article on high altitude propeller design can be found at: http://gltrs.grc.nasa.gov/cgi-bin/GLTRS/browse.pl?1998/TM-1998-206637.html Article referenced is NASA/TM—1998-206637.

Further increasing the main conduit piping size, though costly, may provide an acceptable method to lower system pressure drop.

4.6 Test Cell (General)

The test circuit should be designed to withstand the atmospheric forces against an internal vacuum. Round piping is often the most suitable conduit for this type of service. One material readily used is thick walled PVC piping. Lexan piping could easily be used in the 8" test section. These materials provide very smooth internal non-corrosive surfaces, are easy to work with and are relatively light.

Axial fans originally enclosed in OEM sheet metal would most likely need to be re-installed into PVC piping, should the steel shell not be rated for vacuum service. If non axial blowers are employed a structural assessment of the often flat containment surfaces would need to be conducted.

Depending on the flow conditioning required, more sophisticated flow fields could be constructed. One helpful wind tunnel design link is:
http://navier.stanford.edu/bradshaw/tunnel/index.html

4.7 Conclusions

Advantages and disadvantages of the three configurations investigated are provided below:

Once Through

Advantages: Simple construction, easy to meter flow, low cost of piping.
Disadvantages: Highly inefficient, large vacuum source required, large cost of operation.

Closed Loop Vacuum Pump

Advantages: Simple construction, easy to meter flow, low cost of piping.
Disadvantages: Highly inefficient, large vacuum source required (depending on fluid), high cost of operation, higher cost to obtain and contain working fluid than using air.

Closed Loop Fan

Advantages: Simple construction, low cost of capital equipment, low cost of operation.
Disadvantages: High altitude fan performance needed.

Due to the above, the *Closed Loop Fan* configuration appears to be the most desirable, however, depending upon equipment availability and duration of testing, the other configurations may ultimately prove more beneficial.

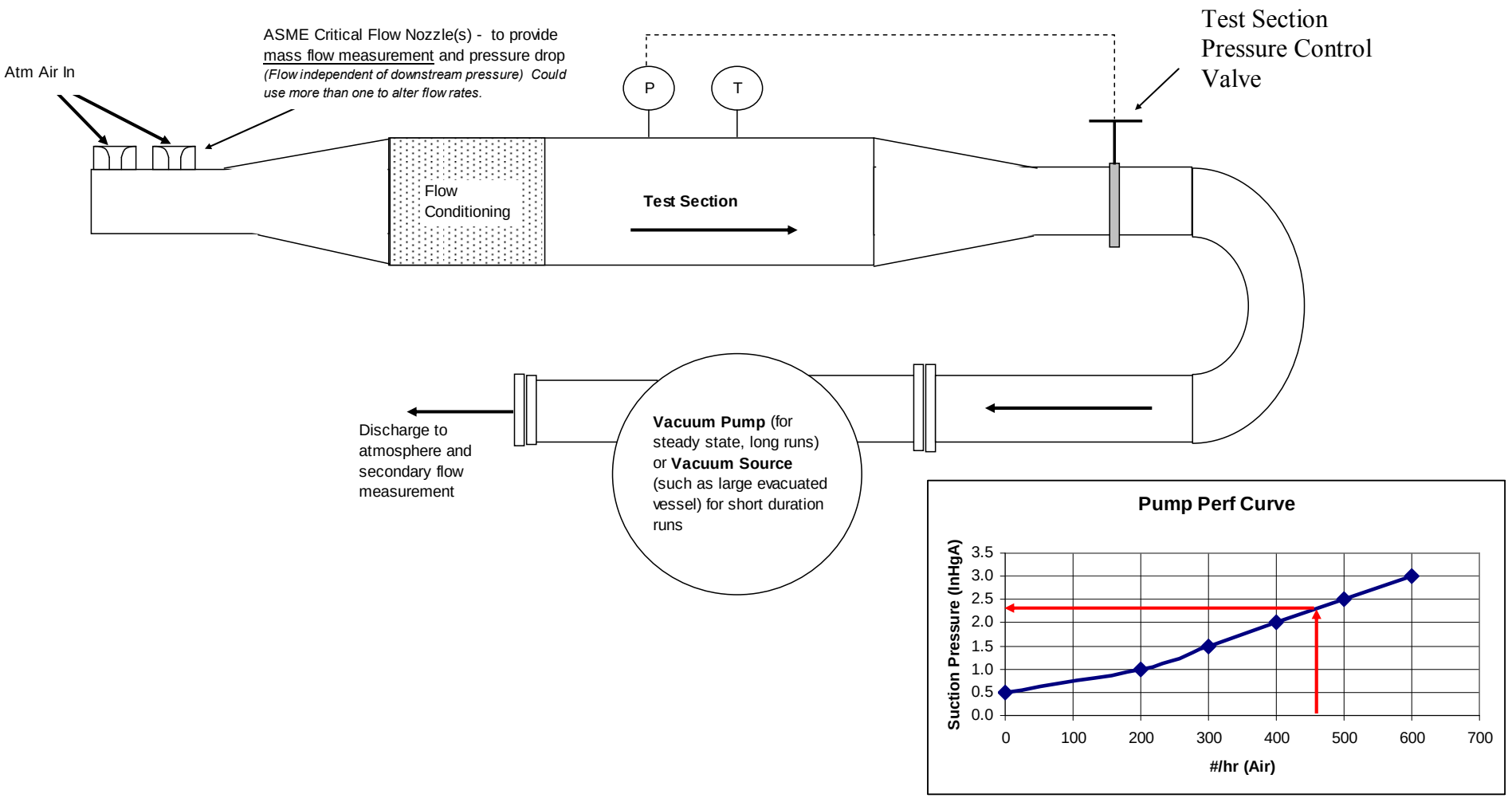

Figure 17: Once through configuration

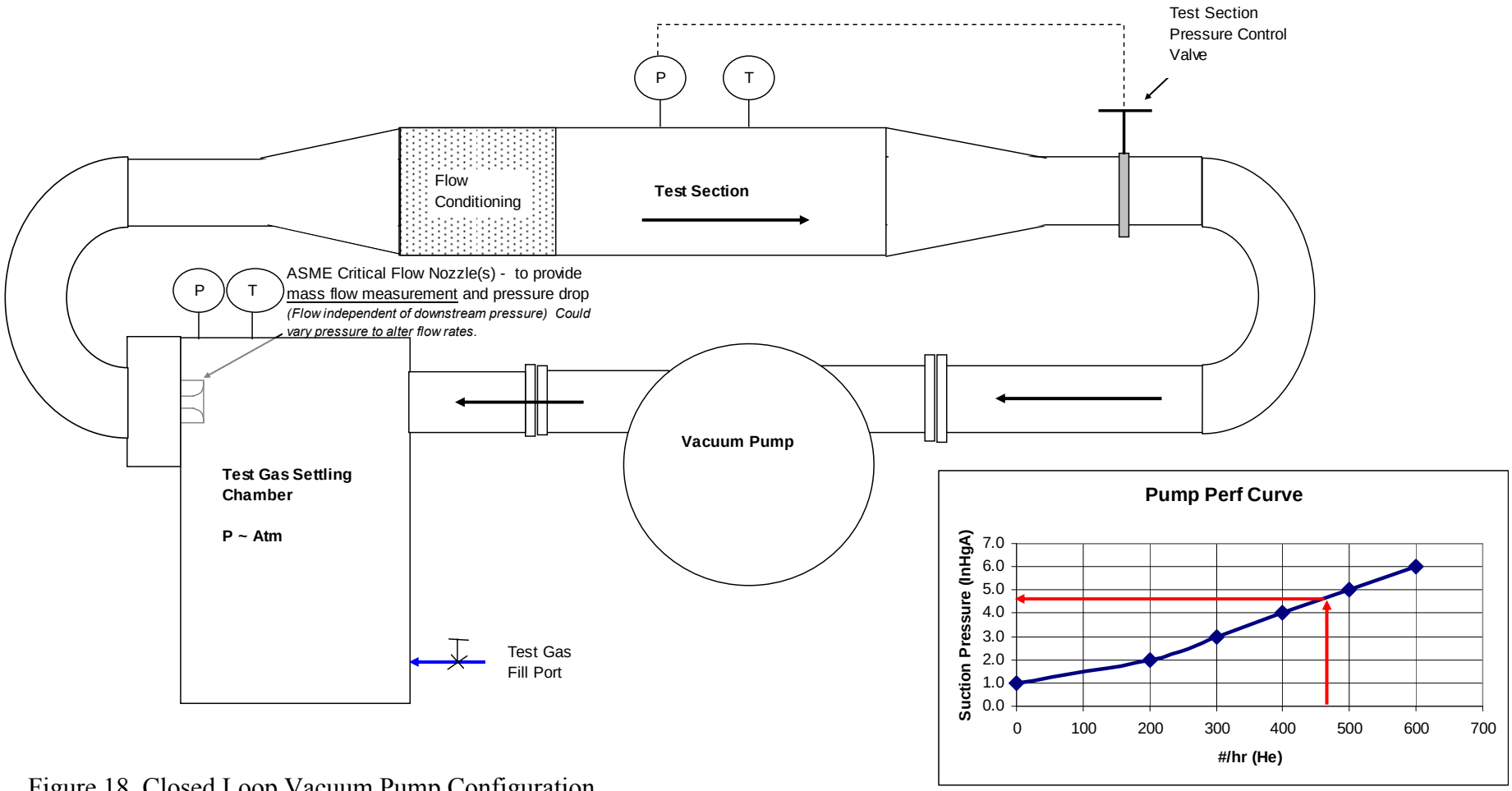

Figure 18. Closed Loop Vacuum Pump Configuration

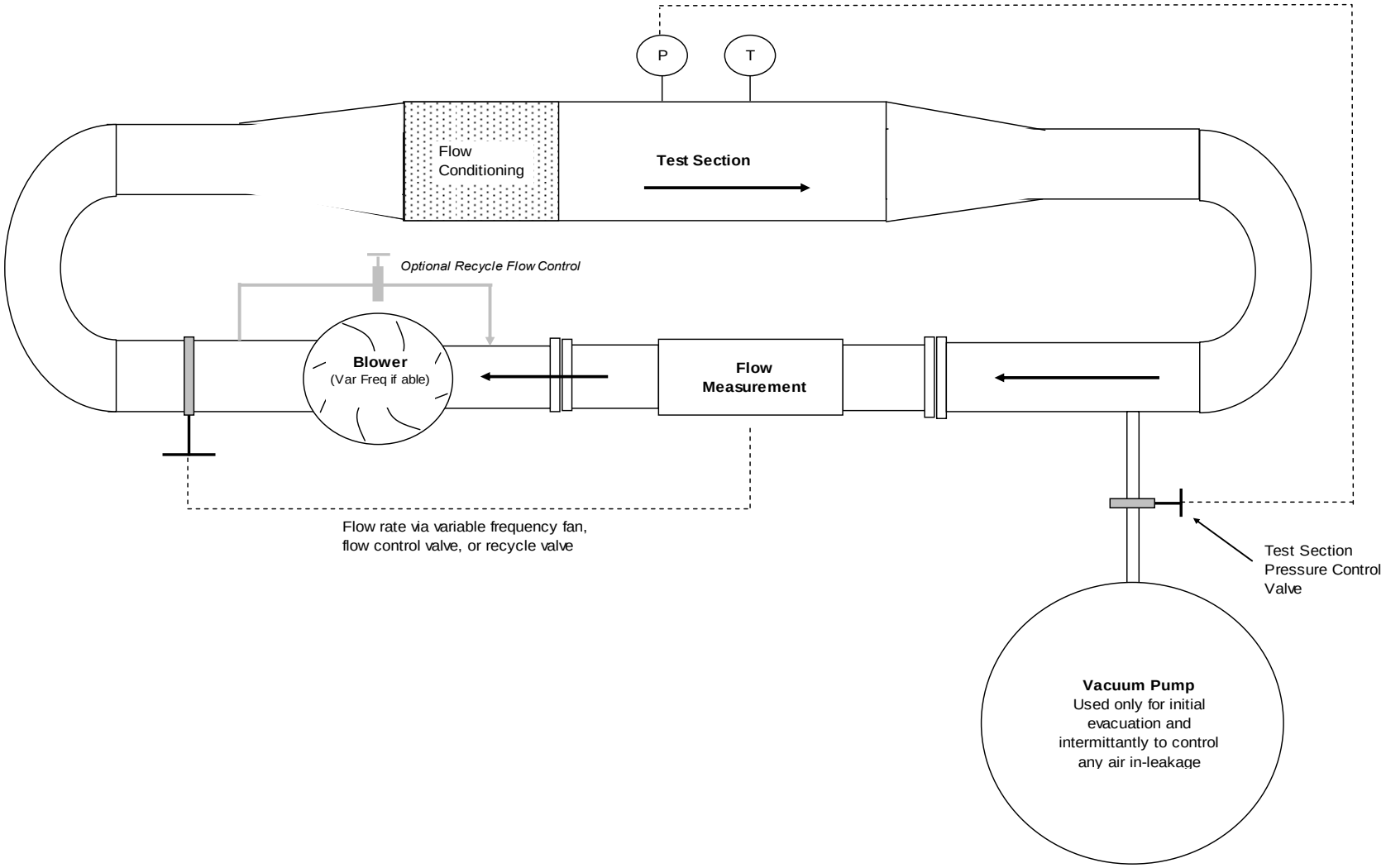

Figure 19. Closed Loop Fan Configuration

5. LOW DENSITY TUNNEL DESIGN AND CONSTRUCTION

5.1 Introduction and Background

Duell returned in the summer of 2006, continuing the work started in the summer of 2005, covered in section 4.3, on high-sensitivity flow measurement instruments for low-density flows. The next step was to design and build a wind tunnel to simulate high-altitude conditions. The first use of this wind tunnel would be to investigate the frequency response of the ionic anemometer and its sensitivity to angle of flow.

Saupe's trade off study, covered in Section 4, concluded that a wind tunnel based on a closed loop fan configuration would be the best design for our purposes. An attempt to obtain an estimate for time and cost of a commercially manufactured tunnel was made with Aerolab; however they declined to bid on the project citing a high volume of projects over the summer and the uniqueness of the request.

This report contains four major sub-sections: planned tasks, which includes the plan for the wind tunnel and subsequent testing; completed tasks, which details what was completed this summer; remaining tasks, which covers what items need to be completed for tunnel operation; and finally future tasks, which contains several recommendations to improve the tunnel and instrument in the future.

5.2 Planned Tasks

The planned tasks for the summer included design of the wind tunnel, analysis of the wind tunnel, acquiring hardware, constructing the tunnel, verifying its operation, and testing the instrument in the tunnel. The design of the tunnel includes everything from the initial determination of the size of the tunnel to the selection of fasteners for securing the fan. The analysis includes both determining the back pressure in the tunnel and the operating temperature of the tunnel. Acquiring hardware consists of both purchasing hardware needed to construct the tunnel, as well as borrowing as much hardware as possible from other personnel and departments. Construction of the tunnel involves the labor of cutting hardware to the correct size and assembling the tunnel. Operational verification includes ensuring that the leaks in the tunnel are not excessive and that it performs as required for testing. Testing the instrument will begin with tests to check its angular and frequency response. During the course of this summer, design, analysis, and acquisition were completed; construction was partially completed; verification and testing have not been started.

5.3 Completed Tasks

This chapter of the report details what has been completed the summer of 2006. The major components of this chapter are design decisions, engineering analysis, electronics, and construction.

5.3.1 Design Decisions

The test section diameter was sized to accommodate the existing ionic anemometer, which is approximately 6 in. long. An 8 in. inner diameter pipe was selected for the test section to avoid significant boundary layer effects. With the desired maximum tunnel wind speed of 30 knots, this creates a required volumetric flow rate of 1060 CFM.

The fan section of the tunnel was sized based on the minimum fan size to provide the desired flow rate. The back pressure, discussed below in Engineering Analysis, proved to be a difficult specification to meet. After some research it was found that a 12” diameter fan could meet the flow and backpressure requirements.

In general the design of the tunnel followed the best practices from literature. Following the best practices from literature, a high aspect ratio (approximately 6) honeycomb screen is used in the tunnel just before the test section to reduce turbulence. One compromise to aid in construction is the omission of screens; while screens improve flow uniformity, the difficulty of mounting them in the tunnel led to their absence.

Another notable deviation from best practices is the design of the diffuser. Diffusers generally expand gradually, often using three legs of the tunnel for expansion, to minimize pressure losses and avoid separation. Due to the difficulty of forming a gradual expansion with PVC, and the amount of labor needed to form the tunnel from sheet metal, it was decided to use a short, tapered PVC connection for expansion. The relatively small expansion ratio, 2.25, partially mitigates the shortcomings of rapid expansion.

Pipe flanges have been placed on both ends of the fan and test sections of the tunnel so they can be removed and accessed relatively easily. Each pipe flange uses a slip ring with four bolts to secure it in place, and a neoprene gasket between the flanges helps to reduce leaks.

The instrument is mounted in the test section using a collar and set screws to attach the instrument to a 1” dia PVC tube. This tube passes through the plug that seals off the test section, and terminates with an elbow and end cap. This allows the tunnel to be sealed off, while allowing the instrument to be rotated for angular response tests. A drawing of the mount is below in Figure 20.

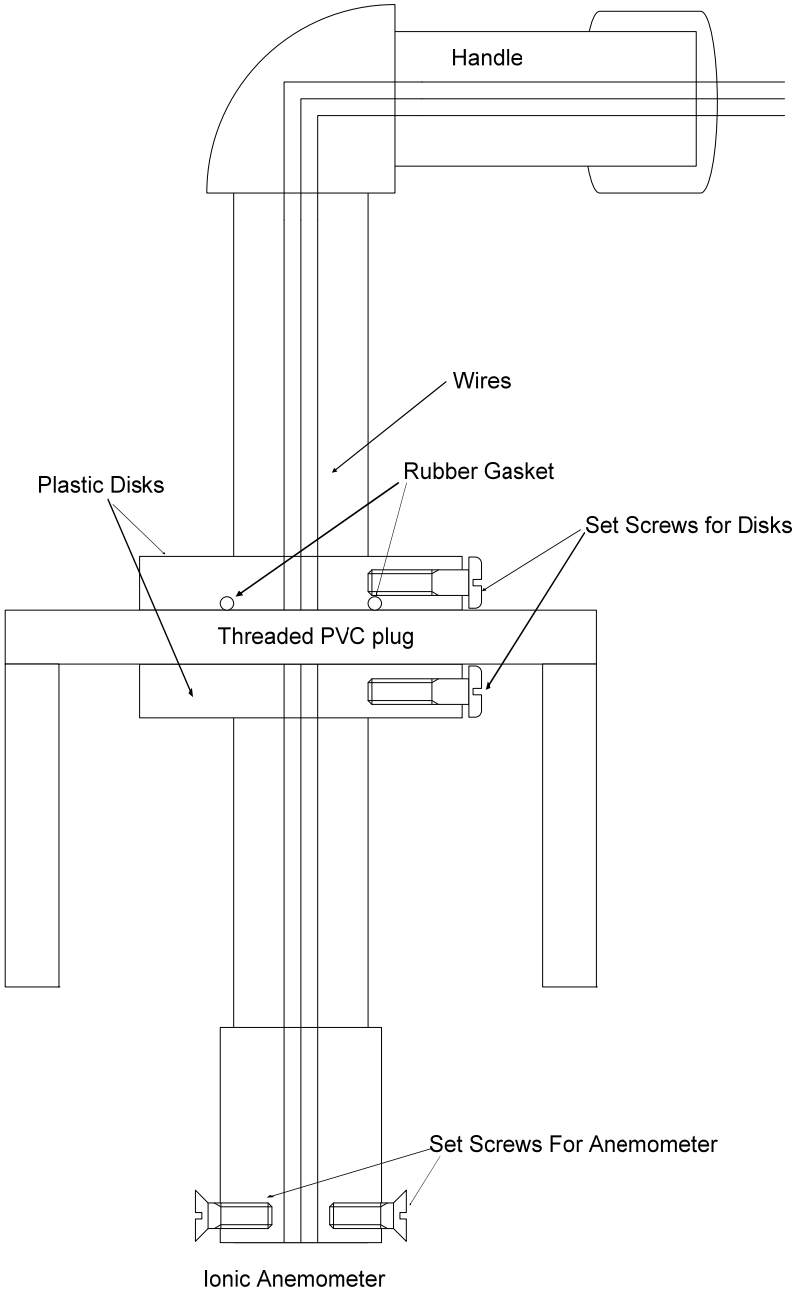

Figure 20. Drawing of Instrument Mount

The vacuum pump is attached to the tunnel via 1" PVC piping. Two ball valves are used; one between the tunnel and the pump and one between the atmosphere and the pump. The valve between the tunnel and pump is used to regulate the amount of air being removed from the tunnel. The second valve to the atmosphere allows some air into the pump so it does not run at no-load for an extended period of time. Several threaded connections have been added to make disassembly, for example for the purpose of changing the distance from the pump to the tunnel, easier. A diagram of the connection is below in Figure 21.

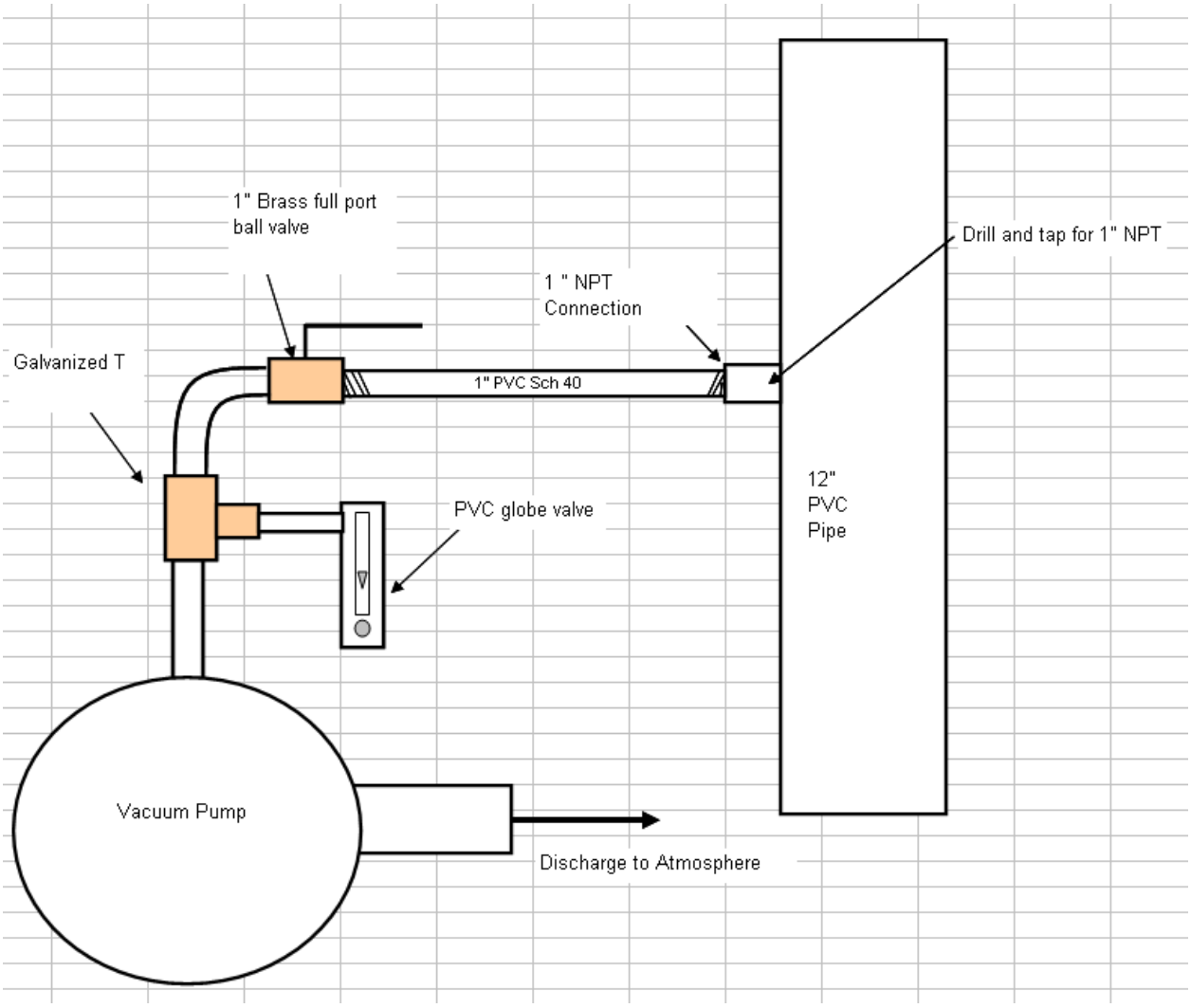

Figure 21. Vacuum Pump Connection

A motor mount was designed to hold the motor and fan in the center of the fan section of the wind tunnel. The mount fits between the motor and the fan due to the position of the mounting holes on an external rotor motor. The motor mount to hold the fan inside the tunnel is shown below in Figure 22.

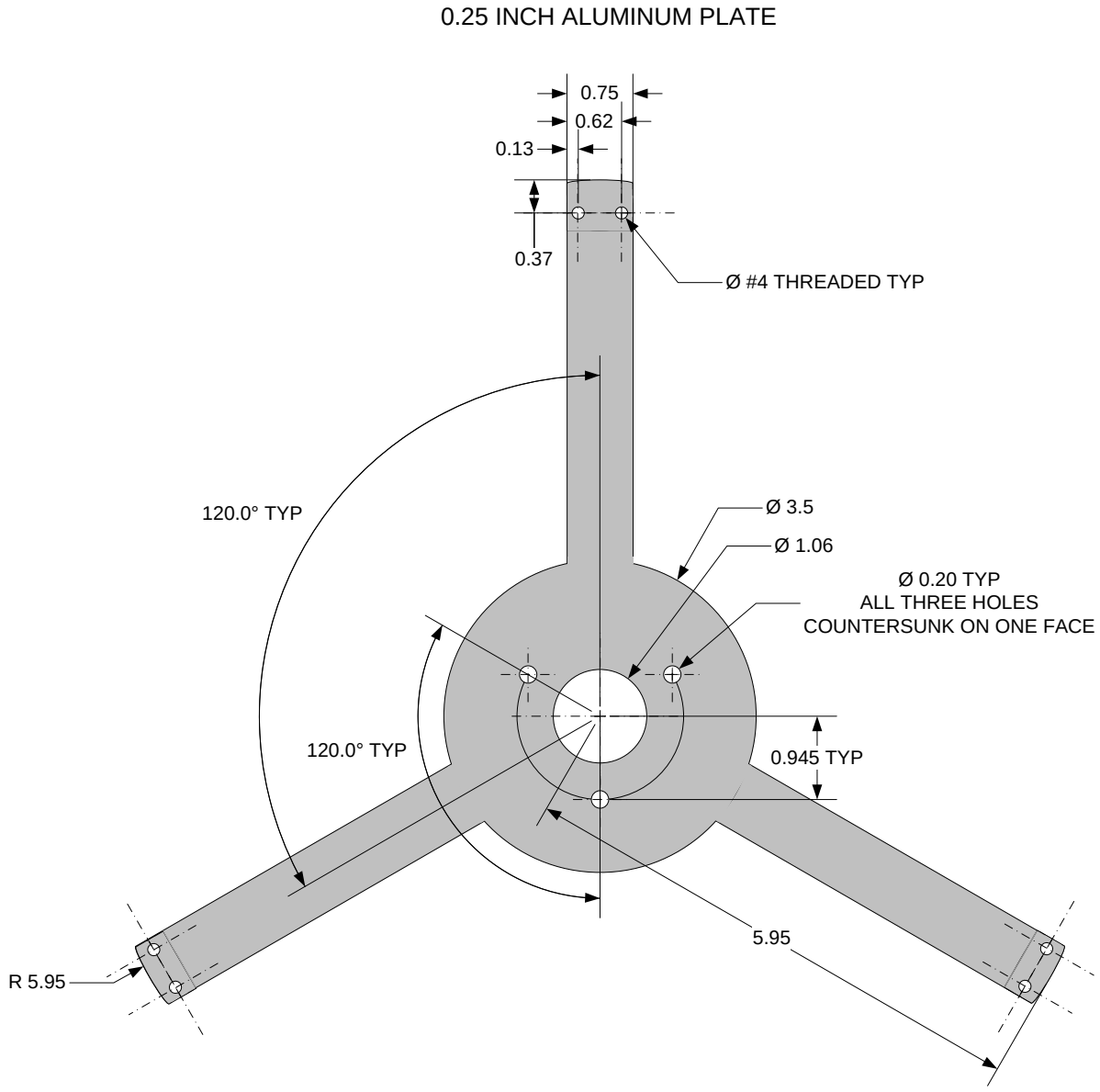

Figure 22. Motor Mount

5.3.2 Engineering Analysis

The first engineering analysis performed on the tunnel was to determine the pressure loss around the tunnel. The worst test case was determined to be a simulation of 55,000 ft at a speed of 30 knots. The back pressure in this case was found to be 0.25 in-H_2O at test density. This is equivalent to approximately 2.9 in-H_2O at sea level conditions, which is how fans are rated. Many commercial providers of HVAC equipment were contacted to attempt to find a fan with these performance characteristics. The ELTA line of fans from Continental Fan was found to be suitable for this application. Following the fan selection, a motor needed to be found to power the fan. The two key requirements are that the motor can vary its power setting within a wide

range, to create a range of speeds within the tunnel, and the motor must be brushless, to avoid potential problems with sparking at low densities. The EC90 brushless flat motor from Maxon Motor was found to be suitable.

The second engineering analysis performed on the tunnel was to determine the operating temperature. There was some concern that the temperature within the tunnel would become excessively warm during prolonged operation. However an analysis of the heat flux through the tunnel walls showed that the temperature inside the tunnel would be just 20 F warmer than outside the tunnel in the worst case (again, 55,000 ft simulation at 30 kts). The actual temperature difference during operation is likely to be even lower, since the cold air leaking into the tunnel will reduce the temperature inside the tunnel.

Heating of the tunnel air was identified as a possible problem. Exchange of heat to the ambient air through natural convection was investigated to determine if any extraordinary measures would be required. Though the thermal conductivity of PVC is quite low, the vast surface area provided by the wind tunnel piping provides a substantial heat transfer surface.

A radial heat transfer model was generated using forced convection on the internal surfaces, conduction through the wall of the piping, and then natural convection to the surrounding air. Internal forced convection was modeled using the classic Dittus-Boelter[14] formulation:

$$\mathrm{Nu} = 0.023\,\mathrm{Re}_D^{\,0.8}\,\mathrm{Pr}^{0.3} \tag{24}$$

Where Nu is the Nusselt number, $\mathrm{Nu} = hD/K$, h is the heat transfer coefficient, D is diameter, and K is the thermal conductivity. Pr is the Prandtl Number, $\mathrm{Pr} = \nu/\alpha$, ν = kinematic viscosity and α = thermal diffusivity. Re is the Reynolds Number, $\mathrm{Re} = VD/\nu$, where V is velocity. Conduction within the pipe sections took the standard cylindrical conduction form:

$$Q_{cond} = \Delta T \left[\frac{\ln r_o / r_i}{2\pi KL} \right]^{-1} \tag{25}$$

Natural convection was modeled using the following relation for externally buoyant convection on a horizontal cylinder[15]:

$$Nu = \left\{ 0.6 + \left[0.38\left(\mathrm{Gr}\,\mathrm{Pr}\right) \Big/ \left[1 + \left(0.559/\mathrm{Pr}\right)^{9/16} \right]^{16/9} \right]^{1/6} \right\}^2 \tag{26}$$

Where

$$Gr = \frac{D^3 g \alpha \Delta T}{\upsilon^2} \tag{27}$$

With a known heat flux through each section of pipe and a dependence upon the temperature difference, ΔT, for the ambient Nu number, an iterative scheme was used to arrive at a complete solution.

The results of this investigation for the heaviest power/thermal loading (55 000 ft), show a 4 degree rise from ambient temperature to the outer pipe wall surface, a nominal increase of 6 degrees across the pipe material itself and another 8 degree rise from the pipe wall inside surface temperature to the bulk fluid flow temperature. This is approximately an 18 degree rise above ambient (or an approximate bulk flowing temperature of 90°F based upon ambient cooling).

If the above calculations are reasonably accurate, no active cooling schemes (i.e. forced air leaks) should be required (though they could be readily employed if needed). Room fans could also be utilized to assist with ambient cooling if needed.

5.3.3 Electronics

To provide usable, recordable, signal levels, current flow induced in the collection rods of the anemometer must be processed utilizing analog signal conditioning electronics. A simple schematic of the circuit is shown in Figure 23. Current from each collector is converted to voltage, and the sum and difference of the voltages are computed utilizing operational amplifier based circuitry. Included in each of these circuits is an offset adjustment to compensate for geometric inconsistencies with probe construction, as well as any electronic input offsets inherent with operational amplifier based circuits.

The sum and difference signals are then amplified to provide appropriate voltage levels allowing maximum resolution from a PC based data acquisition system. Due to the susceptibility of the anemometers' open collectors' to ambient electronic noise; it is also necessary to provide filtering to mitigate signals induced by a laboratory setting (60 Hz noise). In-flight operation away from any AC powered equipment may not require this step. These amplified and filtered signals are then recorded utilizing a 16-bit PC based data acquisition system capable of .3 mV resolution over a +/- 10V input range.

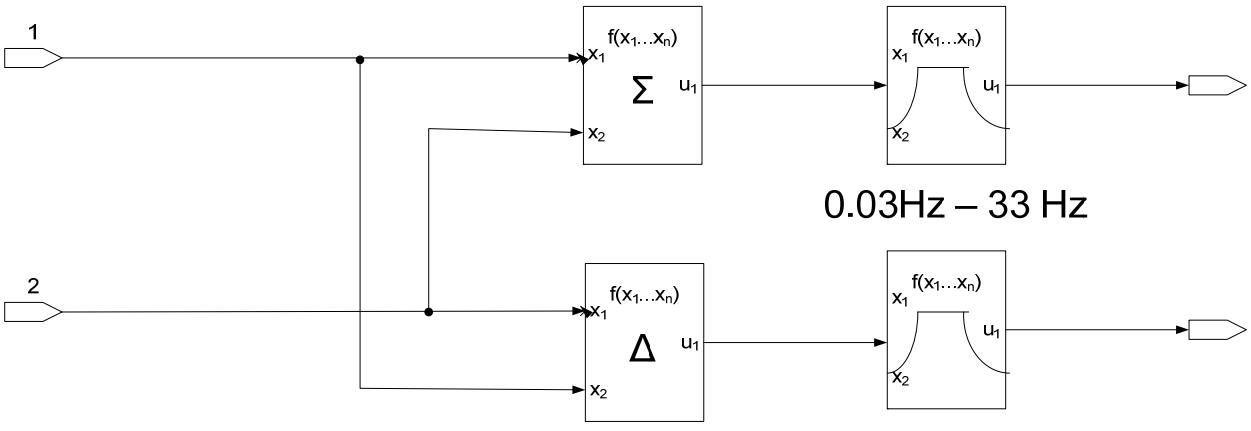

Figure 23. Simple schematic of filtered sum and difference circuit. Current from each collector comes in from the left. The filtered sum is the upper output, the filtered difference on the bottom.

5.4 Low Density Tunnel Construction

The large PVC pipes were cut into sections and the fittings were all attached only as slip fits to facilitate disassembly. An "as-built" drawing of the wind tunnel layout is shown below in Figure 24.

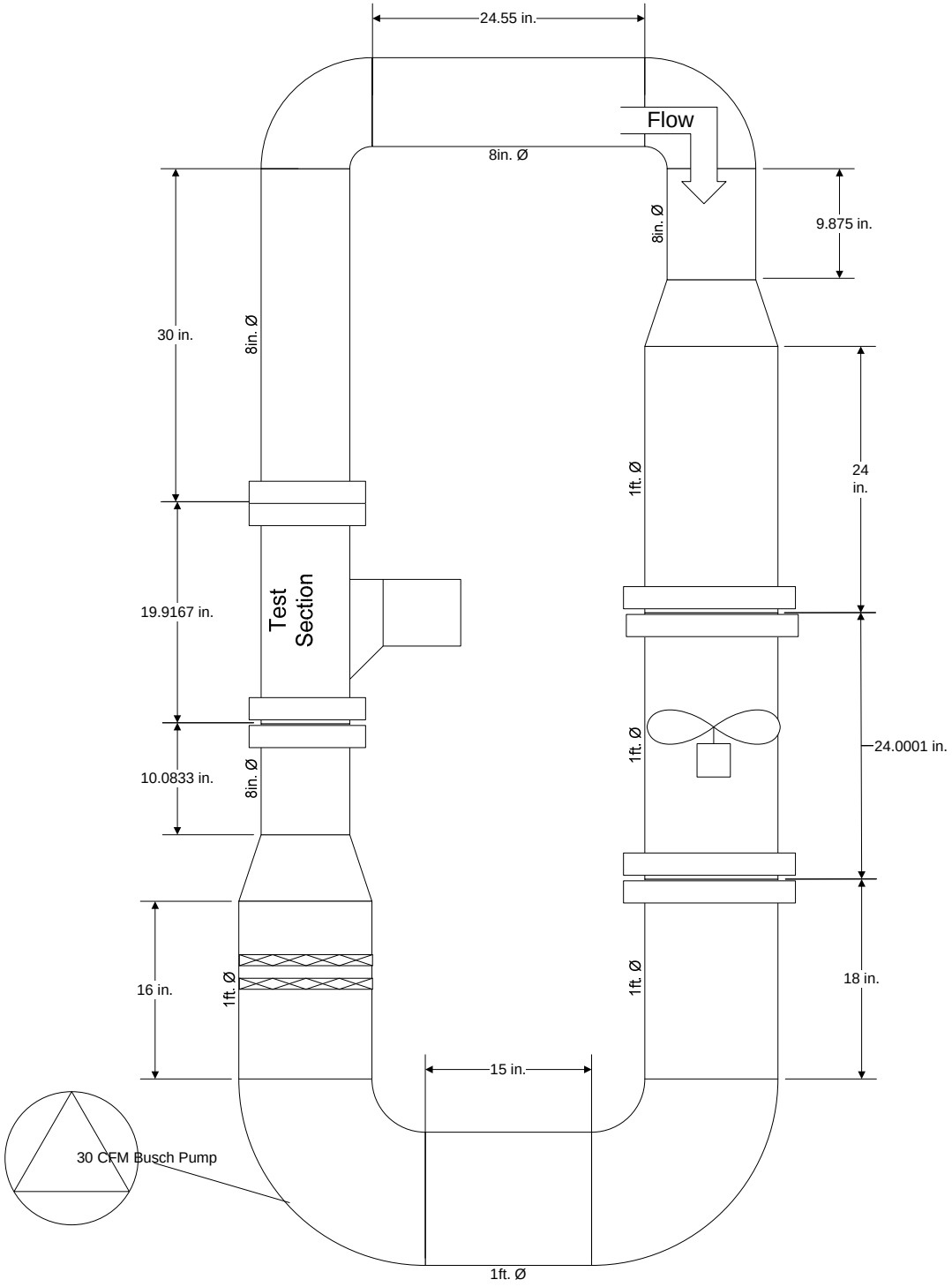

Figure 24. Wind tunnel layout and dimensions

6. TUNNEL INITIAL INSTRUMENTATION CHECK AND TUNNEL CHARACTERIZATION

In December 2006, the wind tunnel was commissioned for sea-level use. The first part of the commissioning process involved assessment and curve fitting of calibration information of pressure and temperature instrumentation.

The two primary pressure instruments utilized were absolute in nature with an applicable range from standard atmospheric pressure (760 mmHgA) down to full vacuum (0 mmHgA). These instruments were checked at near full vacuum (0.01 mmHgA) against an AFRL laboratory vacuum measurement standard. The instruments were then checked against local atmospheric pressure measurement (755 mmHgA), as measured from an AFRL barometric pressure standard. As a cross check, the local atmospheric pressure was compared to the local weather agency reported atmospheric pressure (corrected for lab room elevation and atmospheric temperature). Both methods produced excellent agreement. As the pressure instruments used on the tunnel are designed with a linear response, the full vacuum and atmospheric pressure points were used to create a two point linear calibration curve for each device as shown in Figure 25.

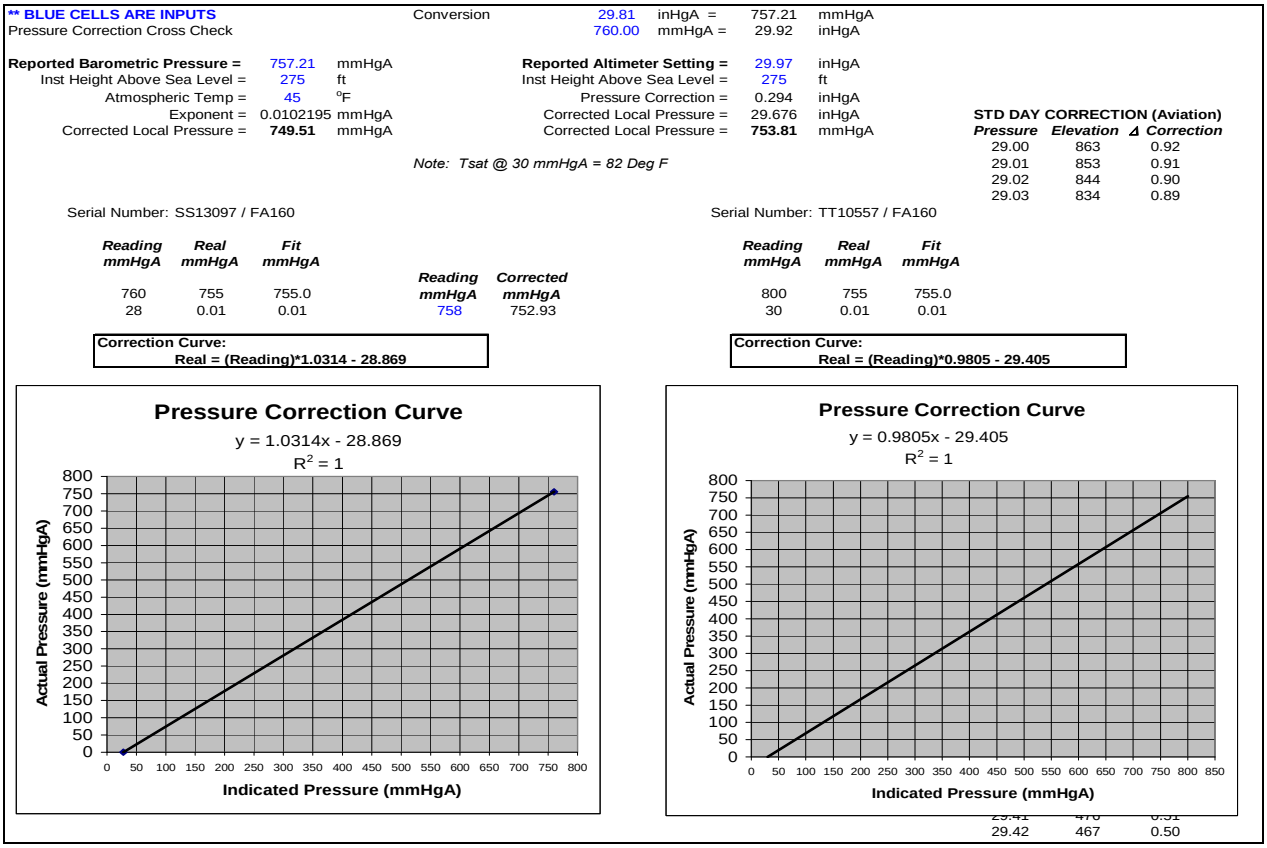

Figure 25. Pressure gage calibration data and curve fits

OMEGA Thermistor

Resistance: 10,000 ohms @ 25°C

10 to 80°C = 50 to 176°F

Conversion Equation

°F =(-5.83475106E-19)*Ohms^5 + (3.36817467E-14)*Ohms^4 - (7.54527227E-10)*Ohms^3 + (8.40899264E-06)*Ohms^2 - (5.22044191E-02)*Ohms + 2.34641272E+02

Ohms	*°C*	*°F*	*°F Fit*
18,790.00	10	50.0	48.97
17,980.00	11	51.8	52.40
17,220.00	12	53.6	54.55
16,490.00	13	55.4	56.12
15,790.00	14	57.2	57.49
15,130.00	15	59.0	58.85
14,500.00	16	60.8	60.31
13,900.00	17	62.6	61.91
13,330.00	18	64.4	63.65
12,790.00	19	66.2	65.49
12,260.00	20	68.0	67.47
11,770.00	21	69.8	69.44
11,290.00	22	71.6	71.48
10,840.00	23	73.4	73.49
10,410.00	24	75.2	75.48
10,000.00	25	77.0	77.44
9,605.00	26	78.8	79.37
9,227.00	27	80.6	81.26
8,867.00	28	82.4	83.10
8,523.00	29	84.2	84.89
8,194.00	30	86.0	86.65
7,880.00	31	87.8	88.37
7,579.00	32	89.6	90.07
7,291.00	33	91.4	91.75
7,016.00	34	93.2	93.41
6,752.00	35	95.0	95.08
6,500.00	36	96.8	96.73
6,258.00	37	98.6	98.40
6,026.00	38	100.4	100.08
5,805.00	39	102.2	101.76
5,592.00	40	104.0	103.47
5,389.00	41	105.8	105.19
5,193.00	42	107.6	106.94
5,006.00	43	109.4	108.70
4,827.00	44	111.2	110.48
4,655.00	45	113.0	112.28
4,489.00	46	114.8	114.11
4,331.00	47	116.6	115.94

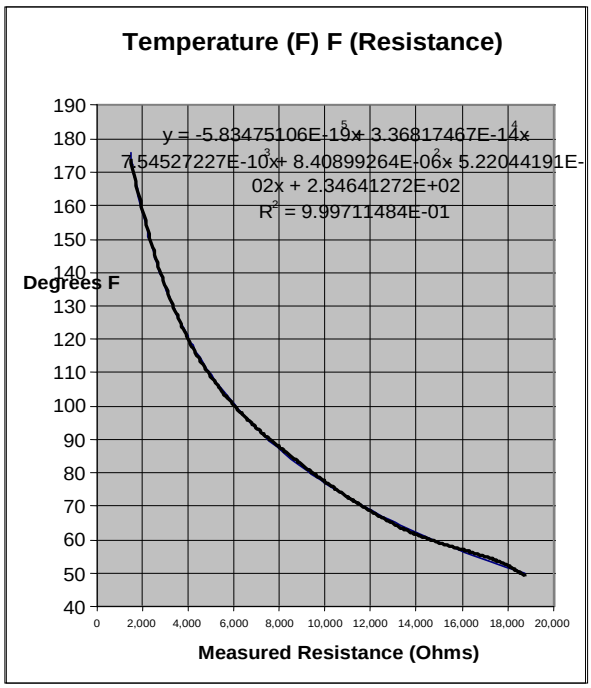

Figure 26. Thermistor calibration

Tunnel temperature was determined using a thermistor. This thermistor was provided with a calibration certificate from the manufacturer, relating temperature (°C) to resistance (ohms) through the use of tabulated data. As the response was highly non-linear, a 5th order polynomial was fit to the data. The details are provided in Figure 6.

Initial runs of the tunnel focused on determining the fan response to tunnel back pressure (effectively trying to calibrate the fan RPM to a measured mean tunnel velocity). During very low density conditions, our velocity check device, a pitot tube, would be of very little use to evaluate tunnel speed (as our Δ pressure instrumentation did not have the accuracy required for such low ΔP operating conditions). Applying fan laws (for density changes) and expected fan curve shifts (for ΔP) would be a basis for determining tunnel velocity at high altitude conditions. Mean tunnel velocity as a function of fan RPM and pressure drop is shown in Figure 27.

Note: First correct CFM based on Back Pressure (new baseline), then correct based on RPM

Sea Level Rated Conditions

CFM =	**1055**	
ΔP =	**2.0**	**in H_2O**
Power =	**253**	**Watts**
RPM =	**3,500**	

20° Blade Angle
@ 3500 RPM

ΔP in H_2O	***CFM***
0.00	2,000
0.50	1,850
1.00	1,700
1.50	1,426
2.00	1,055
2.50	350

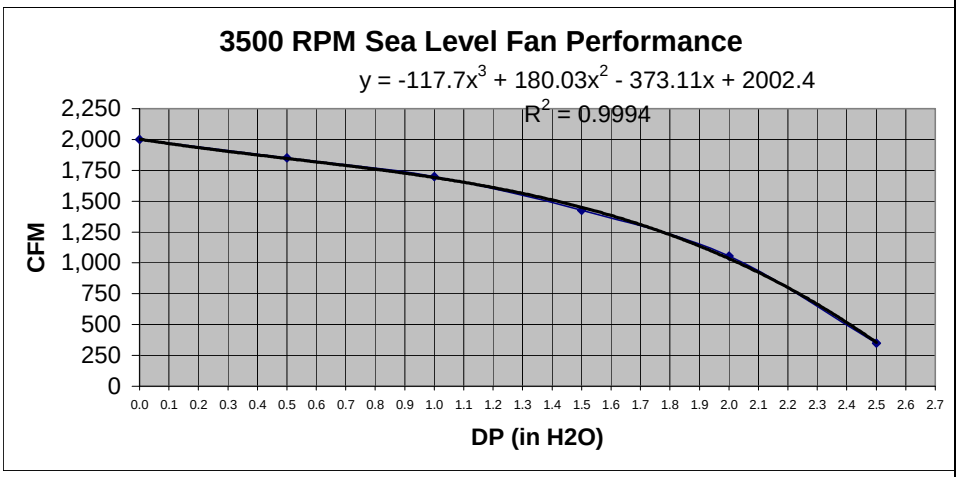

Figure 27. 3500 RPM Sea Level Fan Performance

Initial test run data (provided in Table 4), indicated a large discrepancy between calculated velocity from fan RPM and measured values from the pitot system (~ 45% error). This error was later found to be attributed to an error in calculating fan RPM as a function of reported fan motor frequency (Hz). Tests were re-run to calibrate the tunnel at sea-level using a high accuracy wind turbine meter. A velocity vs fan RPM calibration curve is shown in Figure 28.

Data were later collected at 138 millibars (highest attainable steady state altitude) using fan frequency as the prime indicator of mean tunnel velocity. As accurate pressure drop data was not attained, it has been assumed that the Velocity vs fan RPM calibration curve for sea-level remained valid at 138 millibars.

Table 4: Input for Initial Characterization Run

Date: 18-Dec-06

	TP1	TP2	TP3	TP4	TP5	TP6	TP7	TP8	TP9	TP10	TP11	TP12	TP13
Input Values													
Time	12:20	12:25	12:30	12:35	12:36	13:36	14:36	15:36	16:36	17:36	18:36	19:36	20:36
Trigger Voltage (V)	0.02	0.50	0.98	1.25	1.50	1.95	2.10	2.40	2.70	3.00	3.10	3.52	4.01
Fan Hz	16.00	49.00	88.00	110.00	130.00	165.00	177.00	202.00	225.00	250.00	258.00	291.00	329.00
Driving Voltage (V)	50.00	50.00	50.00	50.00	50.00	50.00	50.00	50.00	50.00	50.00	50.00	50.00	50.00
Driving Amps	0.00	0.01	0.01	0.25	0.20	0.30	0.30	0.40	0.50	0.60	0.70	0.90	1.25
Driving Power (Watts)	0.05	0.50	0.50	12.50	10.00	15.00	15.00	20.00	25.00	30.00	35.00	45.00	62.50
Fan Speed (RPM)	**80**	**245**	**440**	**550**	**650**	**825**	**885**	**1,010**	**1,125**	**1,250**	**1,290**	**1,455**	**1,645**
RPM Based Upon Fan Curve Power	204	439	439	1,284	1,192	1,365	1,365	1,502	1,618	1,719	1,810	1,968	2,196
ΔP Across Fan (inH_2O)	0.00	0.01	0.03	0.05	0.06	0.11	0.12	0.15	0.19	0.24	0.26	0.25	0.35
ΔP Across Pitot (inH_2O)	0.00	0.00	0.01	0.02	0.02	0.03	0.04	0.05	0.06	0.08	0.08	0.10	0.12
Resistance Across Thermistor (Ohms)	11,400	11,440	11,400	11,400	11,400	11,400	11,400	11,400	11,400	11,400	11,400	11,400	11,400
Tunnel Absolute Pressure (mmHgA)	762.0	762.0	762.0	762.0	762.0	762.0	762.0	762.0	762.0	762.0	762.0	762.0	762.0
Output Values													
Fan Curve Volumetric Flow (ft^3/min)	46	140	251	312	368	463	495	562	622	685	705	796	886
Pitot Tube Volumetric Flow (ft^3/min)	0	70	140	177	207	258	279	312	348	388	395	442	488
Corrected Tunnel Pressure (mmHgA)	757.06	757.06	757.06	757.06	757.06	757.06	757.06	757.06	757.06	757.06	757.06	757.06	757.06
Tunnel Temperature (^oF)	71.01	70.83	71.01	71.01	71.01	71.01	71.01	71.01	71.01	71.01	71.01	71.01	71.01
Density (lb/ft^3)	0.0745	0.0745	0.0745	0.0745	0.0745	0.0745	0.0745	0.0745	0.0745	0.0745	0.0745	0.0745	0.0745
8" Flow Area (ft^2)	0.347	0.347	0.347	0.347	0.347	0.347	0.347	0.347	0.347	0.347	0.347	0.347	0.347
Tunnel Velocity (ft/s) Fan	2.20	6.72	12.02	14.98	17.64	22.21	23.77	26.96	29.84	32.86	33.81	38.20	42.53
Tunnel Velocity (ft/s) Pitot	0.00	3.35	6.70	8.48	9.94	12.35	13.40	14.98	16.68	18.59	18.95	21.19	23.40
% Deviation	**N/A**	**50.15**	**44.26**	**43.41**	**43.66**	**44.37**	**43.63**	**44.43**	**44.10**	**43.43**	**43.95**	**44.53**	**44.97**
Viscosity (lb-s/ft^2)	3.83E-07	3.83E-07	3.83E-07	3.83E-07	3.83E-07	3.83E-07	3.83E-07	3.83E-07	3.83E-07	3.83E-07	3.83E-07	3.83E-07	3.83E-07
8" Section Reynolds # (Fan Curve)	8.83E+03	2.70E+04	4.83E+04	6.02E+04	7.09E+04	8.92E+04	9.55E+04	1.08E+05	1.20E+05	1.32E+05	1.36E+05	1.53E+05	1.71E+05
8" Section Reynolds # (Pitot)	0.00E+00	1.35E+04	2.69E+04	3.40E+04	3.99E+04	4.96E+04	5.38E+04	6.02E+04	6.70E+04	7.47E+04	7.61E+04	8.51E+04	9.40E+04
Tunnel Friction Factor (K) (Fan Curve)	N/A	0.00017719	0.000194	0.000201	0.000201	0.000215	0.000209	0.000211	0.000211	0.000223	0.000227	0.000171	0.000191
Tunnel Friction Factor (K) (Pitot)	N/A	0.00071307	0.000624	0.000627	0.000633	0.000694	0.000657	0.000682	0.000675	0.000697	0.000724	0.000557	0.00063
Tunnel Watts (Fan Curve Velocity)	0.000	0.132	0.824	1.650	2.699	5.762	6.866	10.097	13.735	19.389	21.519	23.377	35.918
Tunnel Watts (Pitot Velocity)	0.000	0.066	0.459	0.934	1.520	3.206	3.871	5.611	7.678	10.969	12.062	12.967	19.765

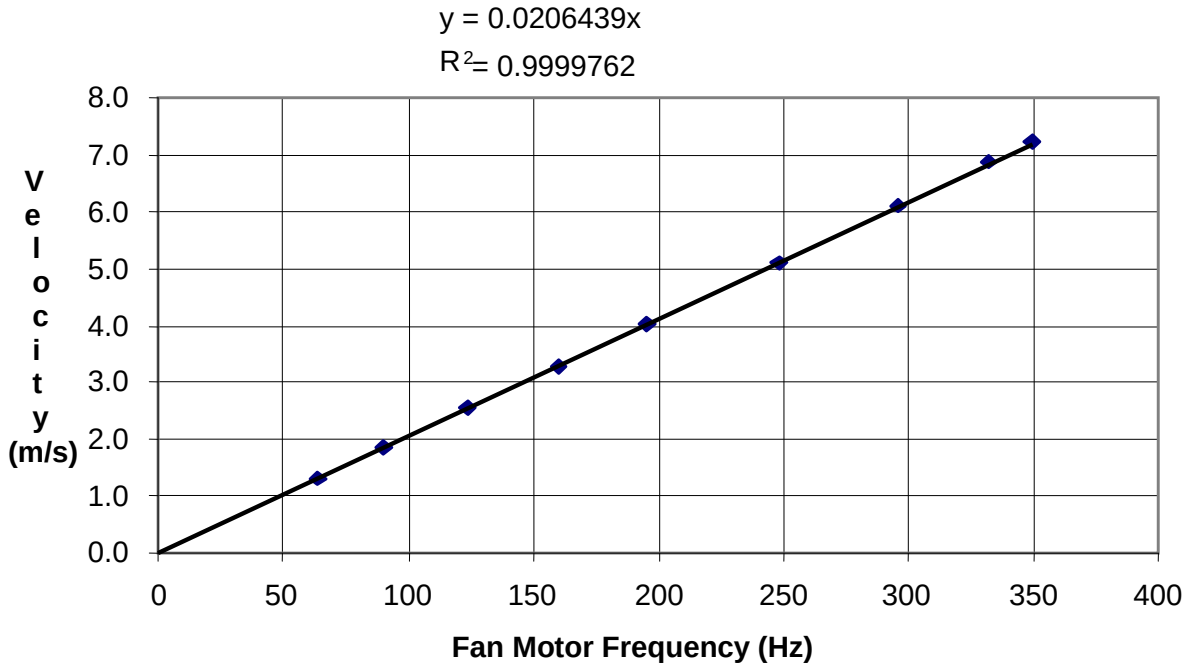

Figure 28. Sea level fan calibration and curve fit

7. IONIC ANEMOMETER ONE-ATMOSPHERE WIND TUNNEL TESTING

The results for our sea-level wind tunnel runs are shown below in Figures 29 and 30. As can be seen in Figure 29, the ratio of the difference current to the sum current of the ionic anemometer increases linearly with windspeed. This is as expected from Equation 23. Figure 30 shows the comparison of the calculated windspeed based on the data collected by the ionic anemometer, and the actual measured windspeed of the tunnel using a conventional propeller anemometer. However, in conducting these tests, the method in which the ionic anemometer data was collected does cause a slight amount of uncertainty. To take a reading at a given windspeed, first the variable input voltage for the fan motor was adjusted to the desired amount. Afterwards, the windspeed was allowed to propagate in the wind tunnel for several seconds until a steady state was achieved. Despite this, there were still small fluctuations in windspeed that

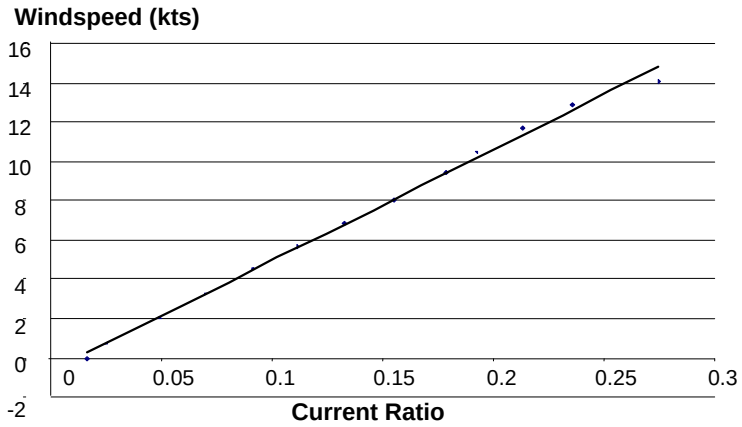

Figure 29. Windspeed deduced from fan speed vs the ratio of collector current difference to collector current sum (Eq. 23) for 1 atmosphere pressure in the wind tunnel.

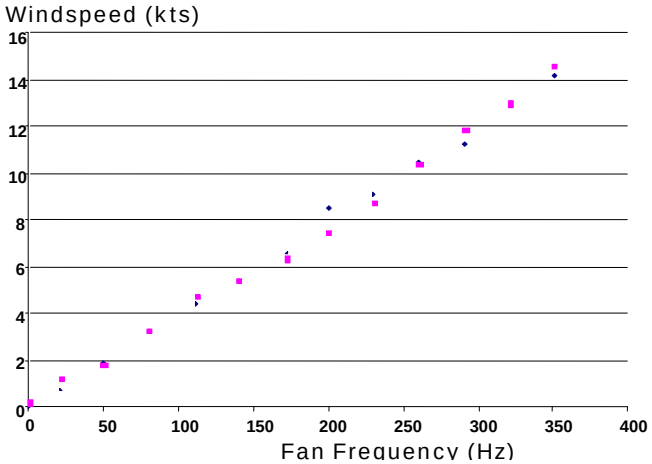

Figure 30. Comparison of windspeed deduced from the calibrated ionic anemometer (blue circles) to the speed measured by a propeller anemometer (pink diamonds), as a function of the Δ/Σ current ratio.

the very sensitive ionic anemometer was able to pick up. The recorded values for the ratios were all *average values* over several seconds while at steady state. This will become more significant during the higher altitude simulations.

8. LOW DENSITY TESTING

The main problem we encountered with the wind tunnel was maintaining a steady pressure for the desired altitude we were simulating. The original plan was to take data at a pressure of 90 millibars. However, this introduced too much uncertainty in our data collection. This uncertainty was primarily caused by small leaks in our system. As mentioned previously, the activation voltage of the ionic anemometer is dependant upon the tunnel density. At much lower pressures, the activation voltage of the anemometer is also much less. The leaks in the tunnel preventing the pressure from maintaining 90 millibars were affecting the readings to the point where we were collecting not only wind velocity perturbations, but also variations due to activation voltage variances. Ultimately, we decided to collect the high altitude data at 138 millibars. This allowed us to simulate high altitude performance while keeping the pressure in the tunnel steady enough to avoid activation voltage uncertainty.

Once it was decided to simulate the high altitudes at 138 millibars, the same windspeed versus ratio test was run. The result of this is shown in Figure 31. While the ratio is still increasing with windspeed, it is not nearly so linear as the one atmosphere test. Even though tunnel pressure was more stable than at 90 millibars, there were enough leaks to make averaging our ratio values over a test run difficult. We collected all data within the range of experienced ratios, but the fact that our activation voltage was still affecting our readings means the error bars are much greater than what would be encountered at sea level. Despite this, the fact that the ionic anemometer was getting increased ratios in such a way with increasing windspeed is very

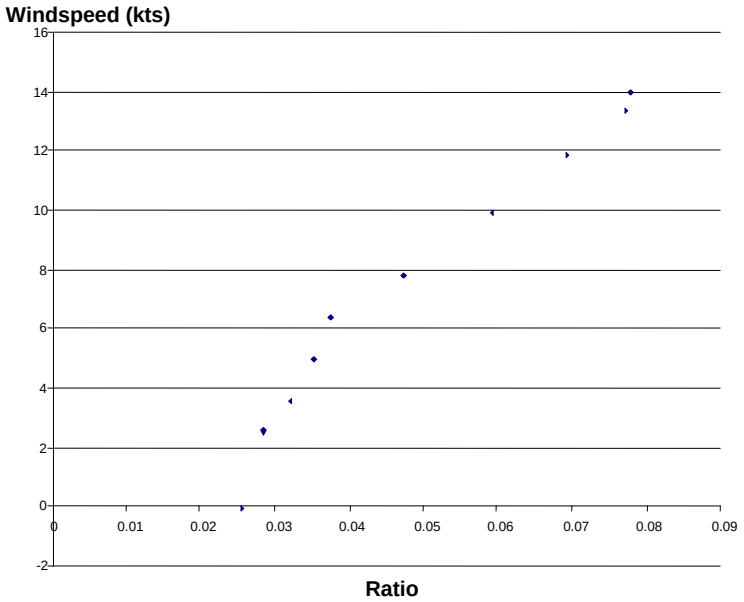

Figure 31. Windspeed based on fan speed vs. Δ/Σ current ratio at 138 millibars

promising for the argument of using it at high altitudes, especially since pressures would be nearly constant for an airship at constant altitude.

The last test was perhaps the most important, actual turbulence measurement. Data was recorded for 8 second periods. The conditions at the time of the data collection were: P = 138 mbars, T = 22^{o}C. This is a density of 0.163kg/m^{3}, which is approximately 16.2 km or 53 000 ft. Due to the presence of turbulent flow in the tunnel, this test not only checked the response time of the ionic anemometer (a major limiting factor of the propeller anemometer), but also provided data to perform statistical analysis. When the ratios were collected, they were converted to the corresponding windspeed in knots as shown in Figure 32, a typical time series. The figure shows over 4000 points of data collected in 8 seconds of testing, with speeds varying from approximately 7.9 to 8.7 knots. Clearly, the ionic anemometer has a very rapid response.

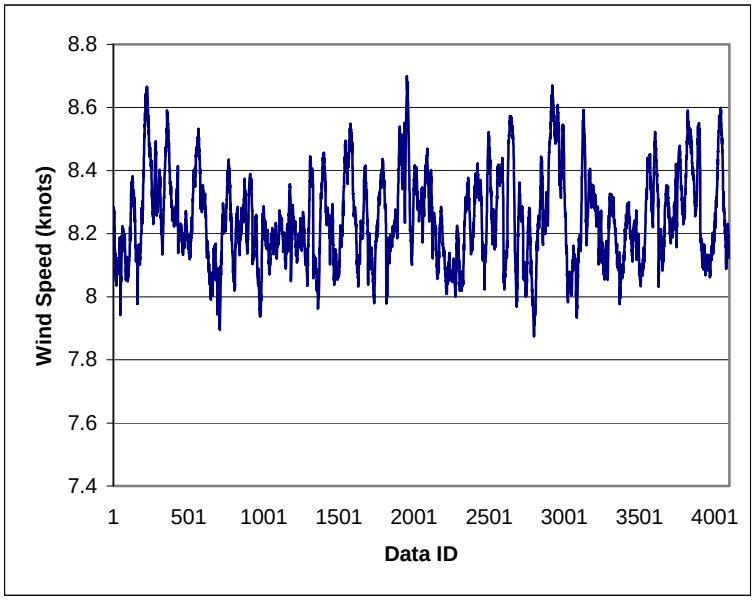

Figure 32. Time series of velocity data from ionic anemometer. The x axis is the number of the sample, the vertical axis is the speed in knots.

9. IONIC ANEMOMETER TURBULENCE ANALYSIS

The data from the ionic anemometer test is essentially a time series of velocity measurements, which can be analyzed for tunnel turbulence levels. The time series is shown in Figure 32. The objective of the analysis was to verify that the turbulence levels were reasonable. Ideally, one would have velocity measurements from a calibrated source to compare to the anemometer output. This was not the case. A hot wire probe would be one such source of data, but a probe that could be installed through the vacuum wall was not available in the time of the run. Instead the anemometer data were subjected to statistical analysis and tested against the reasonableness of the results.

The initial calculations were for mean velocity and the root-mean-square (rms) of the velocity fluctuations. The results of the analysis were that the mean tunnel velocity was 4.24 m/s (8.25 knots), and the rms of the variance (or standard deviation of the measurement) was 0.0738 m/s (0.1435 knots). The ratio of rms to mean velocity gives the turbulence intensity, which is 0.0174 or 1.74%. This is considered to be on the lower end of typical turbulence for large pipes and ventilation flows, which are typically between 1% and 5%.

Next the results were analyzed using power spectral density (PSD) and structure functions. The PSD is defined as the Fourier Transform of the data times its conjugate[16]. The PSD of the velocity data, created using a fast Fourier transform computer algorithm, is shown in Figure 33. The red line is the slope hypothesized by Kolmogorov[17] for the PSD of homogeneous isotropic turbulence for the scales between the outer scale on the low frequency side to the inner scale on the high frequency side. The outer scale is the size of the largest turbulent eddies that form from a disturbance, and the energy of turbulent motion is postulated to be conserved as it cascades down to the inner scale, where the energy begins to be transformed to heat through viscous processes. Also shown is the nominal frequency of a low pass filter used to minimize 60Hz interference known to be present in the laboratory. Data to the right of the filter line should show attenuation, until the noise floor is reached, where the PSD should level out. The transformation from the frequency domain to the spatial domain is accomplished using the mean flow rate of the tunnel, and assuming "frozen flow", i.e. the eddies are assumed to not change as they flow past the sensor. Typically, the PSD for turbulence is plotted as a function of spatial frequency k (m^{-1}), $k = f\,2\pi/\bar{V}$, or about a factor of 1.5 times the temporal frequency values in Figure 33 for our mean velocity of 4.24 m/s.

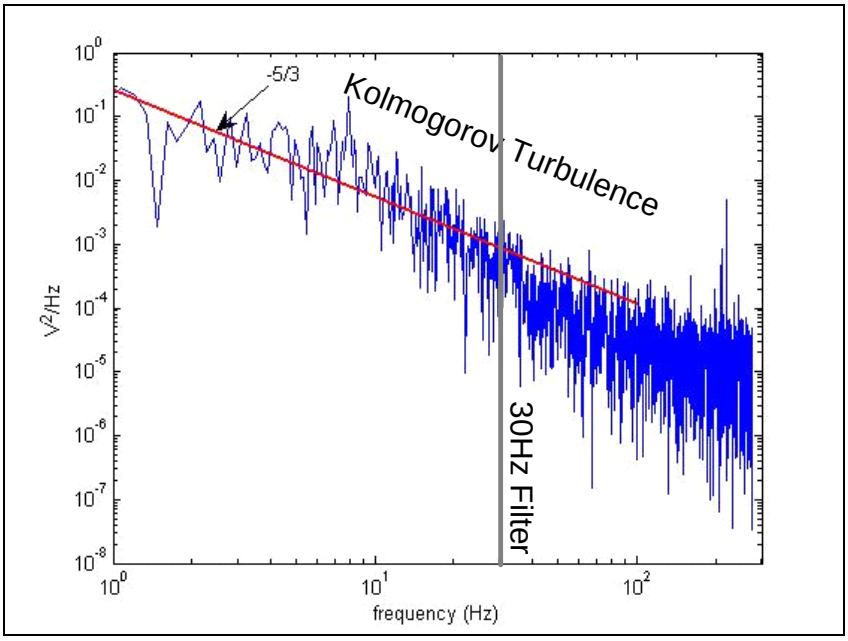

Figure 33. Power Spectral Density (PSD) of the tunnel velocity data from the Ionic Anemometer.

With all the variation in this PSD about all we can say here is that there appears to be a region of Kolmogorov Turbulence in the data. The PSD does seem to show a decrease in energy to the right of the filter line, and suggests that the data become dominated by noise, where the PSD begins to level out above about 100Hz. This is, in fact right about where one would expect to lose information, with a 1cm gap between the electrodes at 4.25 m/s. The right side of the PSD ends at the Nyquist Frequency, which is the highest frequency available given the data acquisition rate, requiring that there is at least two data points per cycle. The outer scale is probably 12 to 8 inches, the pipe diameter before and after the constriction. This translates to a frequency of 20 to 14 Hz, but it does not appear to be an obvious place where the PSD diverges from the Kolmogorov slope.

Structure functions are another common technique used to examine turbulence data[18]. The mathematical definition of a velocity structure function is:

$$D_{UU}(r) = \left\langle \left[U(s) - U(s+r) \right]^2 \right\rangle \tag{28}$$

Where $\langle\ \rangle$ denotes an average over a path s of velocity at two points which are a distance r apart. The Kolmogorov hypothesis when expressed as a structure function becomes:

$$D_{UU}(r) = C_U^2\, r^{2/3} \tag{29}$$

where C_U^2 is the velocity structure constant. The structure function of the velocity data is shown in Figure 34. Note the smoothing effect of the structure function process.

On the larger lengths of the structure function, on the right side, it is clear where the velocity diverges from the Kolmogorov slope when the outer scale is reached. In this case, the outer scale size agrees with the expected order of magnitude of the tunnel diameter, which reduces from .3 m (12 in) to 0.2 m (8 in) immediately before the instrument test section.

The inner scale, where the shear in the eddies is strong enough to begin dissipation into thermal energy, depends on the strength of the turbulence and on the kinematic viscosity of the fluid[19]. From this reference, an approximate formula for the inner scale is

$$l_0 \approx 7.4\left(\nu^3/\varepsilon\right)^{1/4} \tag{30}$$

Where ν is the kinematic viscosity and ε is the kinetic energy dissipation rate, computed using

$$C_U^2 = a\varepsilon^{2/3} \tag{31}$$

where a for this equation is a constant approximately equal to 2. C_U^2 is determined by extrapolating the Kolmogorov segment to the 1m location (i.e. 10^0), where it is approximately $0.025 m^{-(4/3)}/s^2$. Next, using Equation 31, ε is estimated as 0.0013 m^2/s^3. The kinematic viscosity depends weakly on fluid temperature and strongly on density. For our conditions, the viscosity is approximately 8.8×10^{-5} m^2/s., which gives an inner scale of approximately 0.02 m.

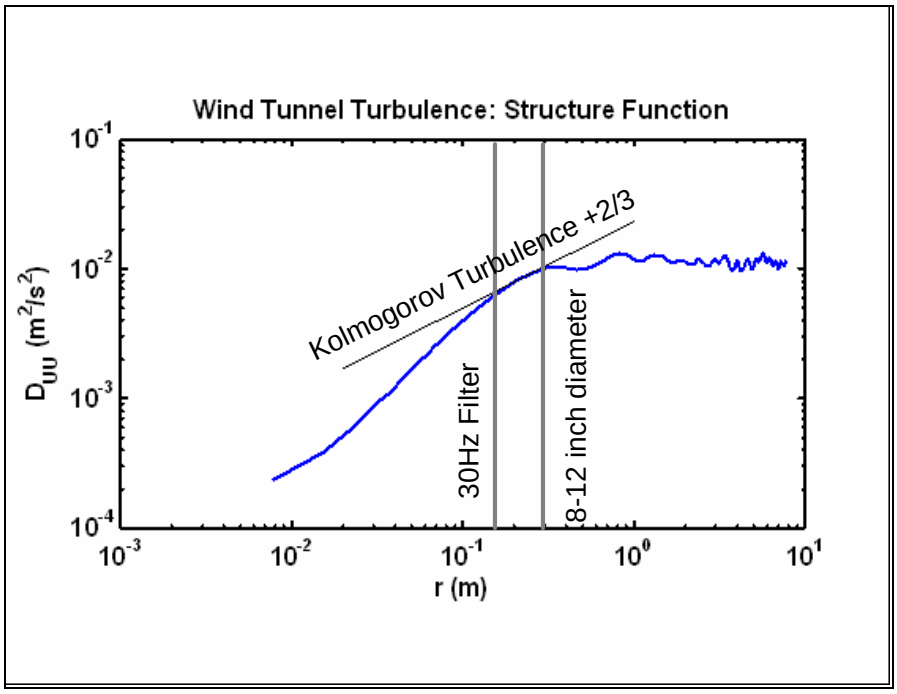

Figure 34. Structure function of the tunnel velocity data from the Ionic Anemometer.

With the structure function manifestation of the time series, it does appear that there is a region of turbulence that follows Kolmogorov's hypothesis from the 30Hz filter to approximately the size of the pipe diameter. Unfortunately, the 30Hz filter blocks the region of the structure function that would have shown us the inner scale, and higher priority laboratory activities prevented further effort on this experiment. With the accumulated information from both PSD and structure function plots, these analyses give us a reasonable confidence that the ionic anemometer is giving accurate velocity fluctuation information.

10. FLIGHT PAYLOAD CONCEPT

Upon completion of instrumentation selection for high altitude operation, packaging and deployment of the atmospheric sensor package (HAA payload) was of prime concern. Figure 36 provides a sketch of the concept. The purpose of the payload is to measure mean temperature, pressure, wind speed and direction, instrument position, velocity, and acceleration at both the HAA altitude and a position of at least 300 m below the airship. The payload will weigh approximately 10 lbs with a power of 30 W at 15 V, will have a data uplink, and have the ability to be deployed and retrieved.

10.1. Requirements

The payload package has many design requirements associated with the atmospheric conditions at airship altitudes – not covered here. Here, we mention those related to data collection and physical design. For the data collection, the driving force of the design is that it must be able to measure three axis mean and fluctuating wind velocities. This will primarily be the ionic anemometer (fluctuating), and propeller anemometer (mean), and their respective support components. The package also must measure mean and fluctuating pressure and temperature. Finally, it must have the ability to resolve relative motion between the payload and the host. For the physical requirements, the first thing to consider is storage and deployment from the host. Ideally, the payload would have an attaching mechanism to allow it to be deployed and retracted directly from the HAA and lowered into position with an expanding

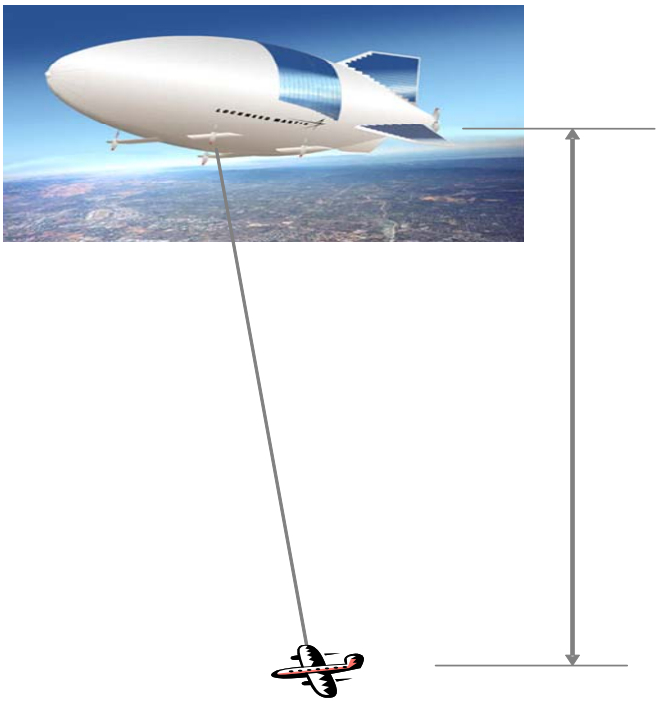

Figure 35. Payload concept for atmospheric turbulence sensor payload suspended below the High Altitude Airship.

(unfolding) structure during deployment using a winching system. The payload would have to be deployed outside of the HAA air stream influence (approximately 300 m).

10.2. Data Storage and Transfer

The payload will be on station for potentially long durations (weeks), so it will be important to have data storage and transfer capabilities. Ultimately, the data collected by the payload will be relayed to the HAA for initial storage and transmission to the user, however, this interface can only be determined once details of a final host system are available and reviewed. Figure 36 shows this relationship.

10.3. Design

We propose that the payload be lowered from the HAA via a thin power/data cable. Attached to this cable would be an interface between the harness that holds the payload and the suspended power cable. Inside this connection mechanism would be housed a data repeater, power supply, media storage and/or IR data interface. To minimize drag and vibration on the suspended cable, a continuous wrap of wire may be necessary to break up shedding vortices should they occur. This wire would be similar to the design currently being used in late model car antennas. A four line harness would be used to connect the platform, to significantly aid the stability on the pitch and roll axis. The most plausible material to use for this harness would be 150 lb Spectra line, which is typical in the performance kite arena, and of which drag would be minimal.

The payload structure resembles an upside down glide, without an elevator. A vertical stabilizer slab would be located on the lower surface empennage to allot the payload to maintain a directional reference with the wind. The wings would have a negative angle of attack, increasing the apparent weight, to help align the payload under the HAA rather than being blown further downstream. The 'fuselage' is circular in cross section and can be used to house instrumentation interfaces, instrumentation power supply, data storage and/or an IR data transmitter and receiver. The payload can be designed in a manner that would allow it to be folded and then auto erected when lowered from the HAA. Front and side views of the payload are shown in Figures 37 and 38.

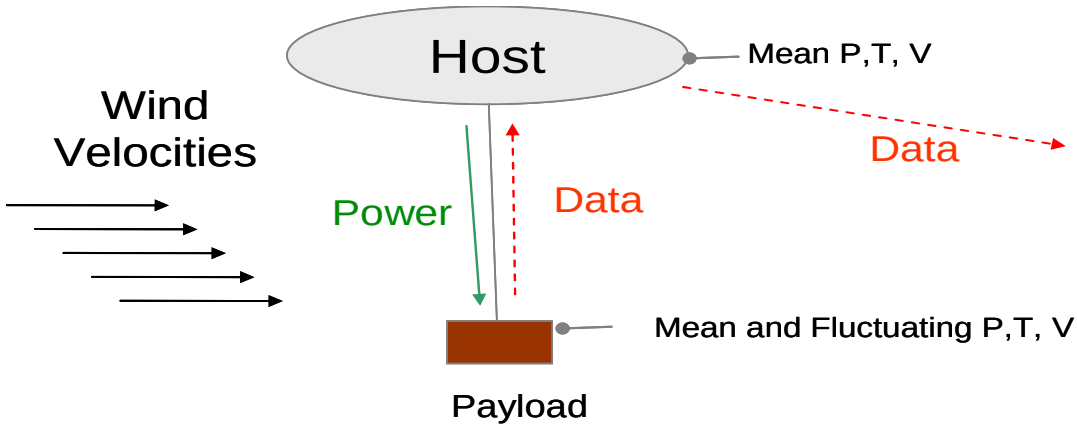

Figure 36. Schematic of Data and Power paths for the atmospheric payload of the HAA or any stratospheric airship.

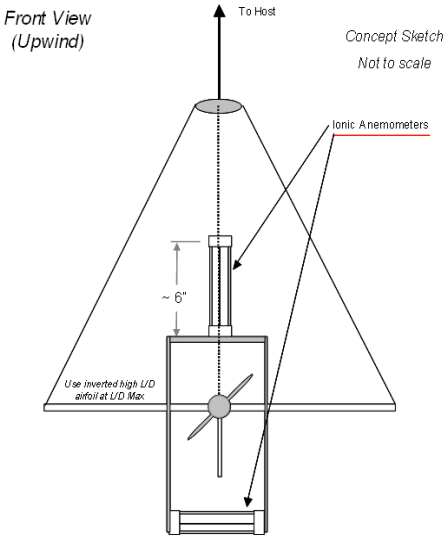

Figure 37. Front view of payload

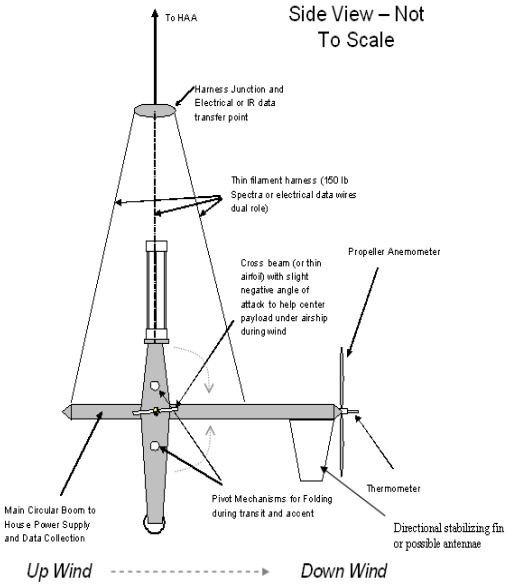

Figure 38. Side view of payload

10.4. Instrumentation

As mentioned in the requirements for the payload, there are many different types of data that must be collected with this payload. The first, and most important, is wind velocity. Fluctuating velocities will be collected from at least two 4-collector ionic anemometers oriented in planes normal to each other, with redundancy in the upstream axis. Mean velocities will be collected from both the ionic anemometers and a propeller anemometer, which will serve as real-time velocity calibration. Temperature will be measured from high accuracy resistance temperature detectors (RTDs), thermistors, and/or thermocouples. The pressure value will be obtained from the HAA's onboard pressure sensors, or included in the payload, space and weight permitting. Finally, absolute position and position relative to the HAA will be obtained utilizing Global Positioning System (GPS) and Inertial Navigation System (INS).

11. CONCLUSIONS AND RECOMMENDATIONS

Measuring velocity fluctuations on a stratospheric airship such as the High Altitude Airship, at high altitude and low speed, is a difficult task for instruments designed to perform that function at sea level and low altitude flight. While variants of the pitot-static probe have been used very successfully at lower altitudes, the combination of low density and low speed results in dynamic pressure differences that are barely detectible, especially for long endurance operational instruments. The propeller anemometer also failed to meet sensitivity requirements. Analysis of a propeller anemometer using blade element theory made clear that the time response of the instrument will be proportional to the product of density and velocity. The HAA environment suffers in the low values of both these parameters. A propeller with very acceptable response at low altitudes loses approximately an order of magnitude in response at HAA altitude density and speeds. Winged vehicles that maintain nearly constant indicated airspeed with altitude would be a better platform for pitot-static and propeller anemometers.

The one anemometer that appears to perform better at higher altitudes is the ionic anemometer. An instrument based on earlier designs of French investigators was built and tested in our laboratory. The 5 to 6kV potentials required to achieve a good ionic flow at near sea level altitudes was reduced to a bit over 1kV at HAA altitudes. In sea level calibration testing, the difference divided by the sum of the ionic currents to the leeward and windward collectors ($\Delta i/\Sigma i$) proved to be quite linear with velocity up to the limits of the wind tunnel, about 6 m/s.

The decision to build an inhouse low density wind tunnel to calibrate the ionic anemometer at HAA operational altitudes proved more of a challenge then originally expected. Problems were compounded by high priority activities in the AFRL shop and laboratories. Consequently fabrication of the device was delayed, and the time available for the test was minimal. In spite of this, the tunnel worked nearly as well as expected. The main problem was leakage, which prevented operation at the simulated design altitude of 60 000 to 65 000 ft. A density representative of 53 000 ft was sustained long enough for the test. Time series of velocity data were collected, and a representative series was analyzed. The information gained by statistical, PSD, and structure function analysis of the data showed that the velocity turbulence data was consistent for the conditions of the test, and appeared to have the levels of time sensitivity attributed to ionic anemometers, which is the detection of eddy sizes down to the size of the gap between the emitter and collector electrodes.

The ionic anemometer instrument appears quite capable of making velocity fluctuation measurements at HAA altitudes. Actual performance has only been verified up to 53 000 ft, and a using agency might demand a simulation up to full design altitude. If higher altitudes are required, a different tunnel must be used, since this appears to be the low pressure limit for this PVC pipe material. Potential users might want to revisit the method used by Barat, which was a variant of the first configuration analyzed in the alternatives, if a suitable vacuum chamber were available as a pressure source. In addition, a notch filter should be used around the 60 Hz laboratory noise source so that higher frequency information such as the inner scale can be investigated in the simulation.

References

[1] Sharman, R., J. Wolff, and G. Weiner, "Description and Evaluation of the Second Generation Graphical Turbulence Forecasting System," *11th Conference on Aviation, Range, and Aerospace*, No. 4.14, 2004.

[1] Scorer, R.S., "Theory of Airflow Over Mountains: II – The Flow Over A Ridge," *Quarterly Journal of the Royal Meteorological Society*, Vol. 79, 1953.

[1] Bacmeister, J.T., P.A. Newman, B.L. Gary, and K.R. Chan, "An Algorithm for Forecasting Mountain Wave-Related Turbulence in the Stratosphere", Weather and Forecasting, Vol. 9, June 1994, pp. 241-253.

[1] HAA Program Description on the Lockheed Martin web site: http://www.lockheedmartin.com/products/HighAltitudeAirship/index.html

[1] USASMDC, "HAA: High Altitude Airship," Huntsville, Alabama, Space and Missile Defense Battle Lab, accessed at http://www.smdc.army.mil, Sep 2004, cited by L. Jamison, G.S. Sommer, and I.R. Porch III, "High-Altitude Airships for the Future Force Army", Rand Arroyo Center, Santa Monica, CA, 2005

[1] Lomas, C.G., *Fundamentals of Hot Wire Anemometry*, Cambridge University Press, Cambridge, 1986, pp 62 – 66, and p. 155.

[1] MATLAB® and Simulink®, Registered trademark of The Mathworks, 3 Apple Hill Drive, Natick, MA 01760-2098 (www.mathworks.com).

[1] Glauert, H., *The Elements of Aerofoil and Airscrew Theory*, 2nd Edition, Cambridge University Press, New York, 1947, Chapt.XVI.

[1] R.M. Young Company, 2801 Aero Park Drive, Traverse City, Michigan 49686, (www.youngusa.com)

[1] Barat, J., "Some characteristics of clear air turbulence in the middle atmosphere", *J. Atmos. Sci.*, 39, 2553-2564, 1982.

[1] *U.S. Standard Atmosphere, 1976* (NOAA, NASA) Washington, D.C. 1976

[1] *Standards for Steam Jet Vacuum Systems 5th ed., 2000* Heat Exchange Institute (HEI), http://www.heatexchange.org/pub/default.htm

[1] *Vacworks II* (Vacuum system sizing public use software). Graham Corporation, Batavia, NY. http://www.graham-mfg.com

[1] Holman, J. P., *Heat Transfer*, McGraw-Hill Book Company, New York, 3rd Edition, p. 176.

[1] F. P. Incropera and D. C. DeWitt, *Fundamentals of Heat and Mass Transfer*, John Wiley & Sons, Inc., 1985, p. 435.

[1] Burington, R.S., Handbook of Mathematical Tables and Formulas", McGraw – Hill Book Company, New York, NY, 5th Edition, 1973, p. 227.

[1] Kolmogorov, A.N., "The local structure of turbulence in incompressible viscous fluid for very large Reynolds numbers", a translation by V. Levin in *Proc. R. Soc. Lond.* A (1991) 434, 9 – 13, of an article originally published in Russian in *Dok. Akad. Nauk SSSR*, 30, 4 (1941)

[1] Frehlich, Rod and Robert Sharman, "Estimates of turbulence from numerical prediction model output with applications to turbulence diagnosis and data assimilation", *Monthly Weather Review*, Vol. 132, p. 2308-2324, 2004.

[1] Hocking, W.K., "Measurement of turbulent energy dissipation rates in the middle atmosphere by radar techniques: A review", *Radio Science*, Vol. 20, No. 6, pp 1403-1422, 1985.

Appendix A: High Altitude Wind Tunnel Start-up Instructions and Instrumentation List

The following outlines the instrumentation and general procedure required for the successful start-up and operation of the locally fabricated high altitude wind tunnel at AFRL Hanscom AFB, MA.

It is highly recommended that all instrumentation be validated as operational and accurate utilizing ambient atmospheric pressure prior to initiating a vacuum source (to arrive at desired altitude).

Table A1: Wind tunnel Monitoring Instruments (for locations, see Figure A1)

Nomenclature	Method	Measurement	Range
ΔP1	Pitot Tube / DAQ	Velocity via ΔP	0-1.0 inH_2O
ΔP2	DAQ / Manual	Tunnel ΔP	0-2.0 inH_2O
P1	DAQ / Manual	Tunnel Mean P	0-760 mmHgA
P2	DAQ / Manual	Vacuum Pump P	0-760 mmHgA
T1	DAQ / Manual	Tunnel Mean T	50-150 Deg F
RPM	DAQ	Fan Speed	As Required
VOLT	DAQ	Fan Voltage	As Required
AMP	DAQ	Fan Current	As Required

Atmospheric Checkout

Initial check out of tunnel operation and instrumentation should be accomplished at ambient sea level conditions if possible.

1. With the tunnel fully instrumented and data acquisition system active, static values of all instrumentation should be checked for operation against known zero flow calibration conditions (that is ΔP's = 0, T1 = Ambient, P1 = Ambient, VOLT = 0, RPM=0 etc.).
2. Fan shall be placed in operation and rotational velocity slowly increased to 2,800 RPM. At this point, tunnel values should be at or near the values provided in Table A2.
3. If measured values are not in agreement with Table A2, system should be investigated to determine the cause.
4. Closely monitor tunnel temperature T1. If T1 exceeds 150 ^oF, fan shall be shut down until system cools to acceptable levels.

Table A2: Initial Conditions for Sea Level Checkout

Nomenclature	Raw Value	Calculated Value	Ultimate Calculated Result
ΔP1	0.57 inH_2O	50 ft/s	Velocity
ΔP2	1.31 inH_20	1.31 inH_2O	Tunnel Loss Efficiency
P1	~760 mmHgA	~760 mmHgA	Air Density (altitude)
P2	~760 mmHgA	~760 mmHgA	Air In-leakage Validation
T1	~70 ^oF	~70 ^oF	Air Density (altitude)
RPM	2,833	1,055 Ft^3/min	Volumetric Flow (velocity)
VOLT	TBD	270 Watts	Tunnel Input Power
AMP	TBD	270 Watts	Tunnel Input Power

Note:

- Due to the much higher Power requirements of the fan motor at high density (low altitude) conditions, heat rejection to the tunnel will be several times greater than during low density (high altitude) operation. Therefore, tunnel mean temperature T1, should be closely monitored and controlled (using cooling air bleed if needed). Should this value exceed 150 ^oF, tunnel should be shut down and allowed to cool sufficiently prior to further use.

- Due to the very low ΔP's involved, VERY accurate measurements will be required for these values. Recommend angled water manometer for a manual cross check of tunnel ΔP's and pitot tube measurements.

Initial Checkout at Altitude

Once system has been validated under sea level conditions, tunnel can be slowly brought to high altitude conditions as follows:

1. Ensure fan is not in motion.
2. Ensure valve V1 is closed and that valve V2 is fully open.
3. Start vacuum pump.
4. Slowly open tunnel isolation valve V1 while monitoring tunnel pressure P1.
5. Slowly begin to close pump bleed valve V2 while monitoring tunnel pressure P1.
6. Continue to slowly close V2 until the desired pressure is obtained (~74 mmHgA)
7. Adjust V2 to maintain optimum pressure throughout the run cycle.
8. If tunnel pressure remains above 74 mmHgA with V2 fully closed, investigate system for air in-leakage and correct. Note: Pump performance curve (Figure A5) can be used to determine the actual magnitude of air in-leakage.
9. Start fan and adjust rotational velocity to 3,500 RPM
10. Adjust fan RPM to obtain desired flow velocity. If flow velocity is not attained by 4,500 RPM discontinue test and increase blade angle by 10^o.

11. Compare measured values to those provided in Table A3. Significant deviations should be noted and investigated.

12. Closely monitor tunnel temperature T1. If T1 increases beyond 150 ^{o}F, an artificial air leak should be introduced just downstream of the 8" test section (by opening and adjusting valve V3) to cool the main flow.

Table A3: Initial Conditions for 60 000 ft simulation

Nomenclature	Raw Value	Calculated Value	Ultimate Calculated Result
ΔP1	**0.06 inH_2O**	50 ft/s	Velocity
ΔP2	0.21 inH_20	0.21 inH_2O	Tunnel Loss Efficiency
P1	74 mmHgA	74 mmHgA	Air Density (altitude)
P2	< 74 mmHgA	< 74 mmHgA	Air In-leakage Validation
T1	70 ^{o}F	70 ^{o}F	Air Density (altitude)
RPM	3,500	1055 Ft^3/min	Volumetric Flow (velocity)
VOLT	TBD	80 Watts	Tunnel Input Power
AMP	TBD	80 Watts	Tunnel Input Power

Note:

- As tunnel pressure decreases it is important to closely monitor fan RPM as an inadvertent overspeed due to the lowering density conditions could cause damage to the blades, tunnel walls or drive motor.

- Due to the very low densities involved, VERY accurate pitot tube measurements will be required for a velocity calculation. Recommend angled water manometer for a manual cross check of tunnel ΔP's.

- The above set pressure of 74 mmHgA assumes a mean air temperature of 70 ^{o}F. The required pressure will increase as cell temperature increases. See Section 4.3 in body of technical report for discussion and plot of required pressure.

- Final fan blade angle and RPM will require iterative testing once system has been check-out on-line at altitude. If unable to obtain required volumetric flow(velocity) increase RPM (up to a maximum of 4,500). If still unable to generate enough flow increase blade angle in increments of 10^0 until flow is obtained

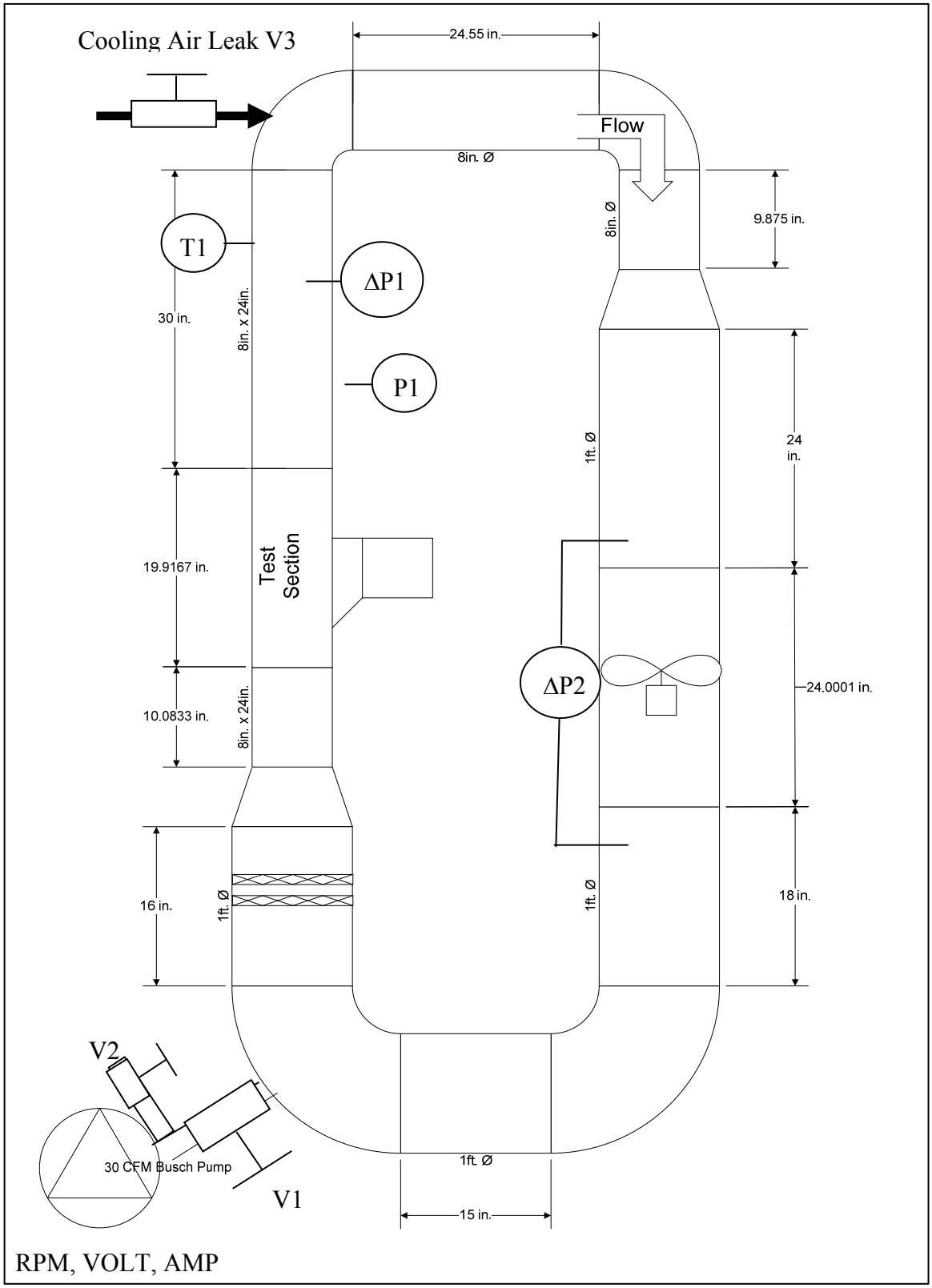

Figure A1. Schematic of wind tunnel showing locations of instruments described in Tables A1, A2, and A3.

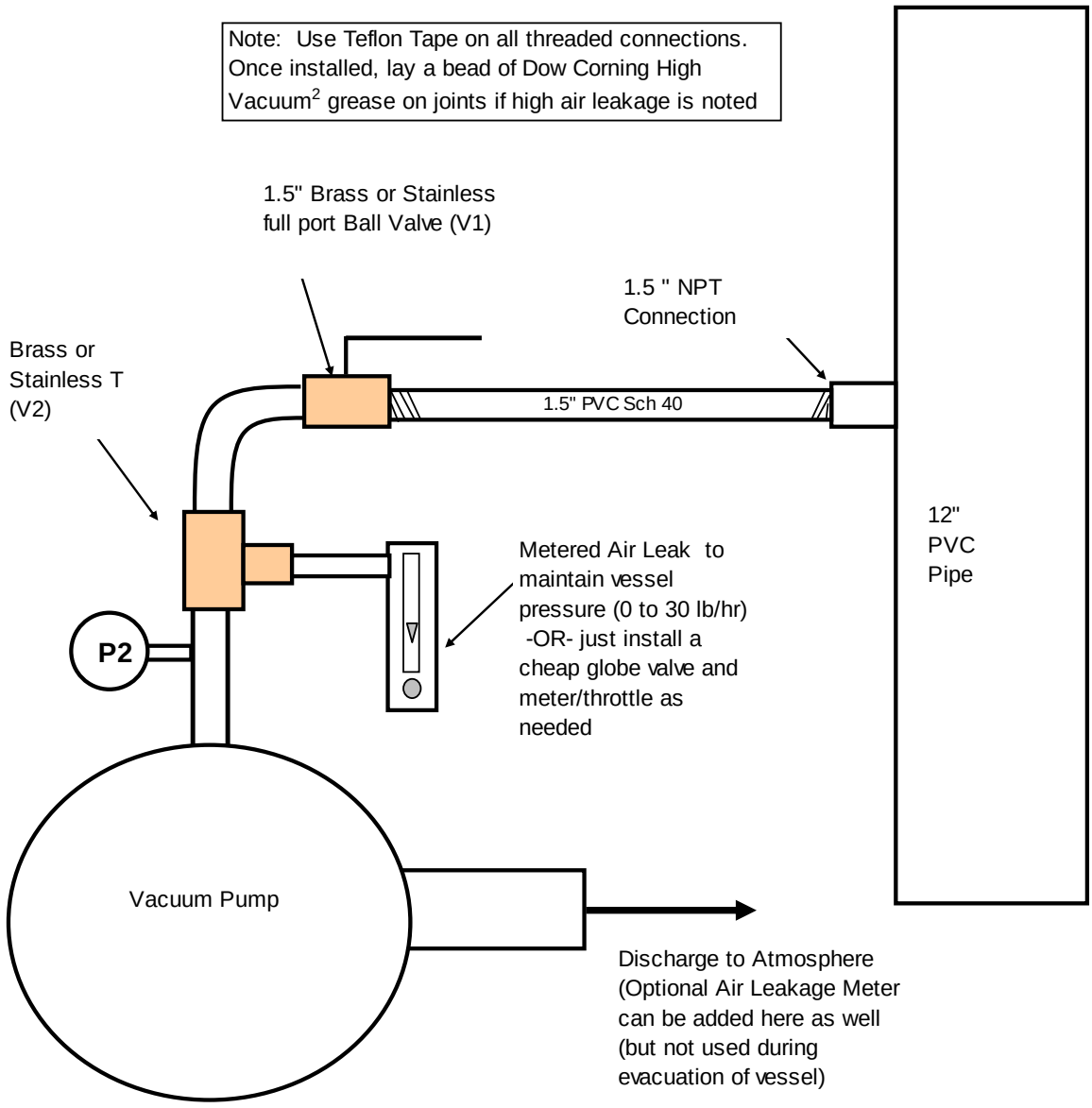

Figure A2. Vacuum pump installation detail

Fan Code: **012/150/5/10**

Requirements

Volume:	1000 cfm
Static Pressure:	1 "WG
Selection Pressure:	1.12 "WG at std conditions
Installation Category:	TYPE D
Temperature:	70 deg F
Altitude:	0 ft

Fan Data (at STP)

Type:	Axial Impeller
Diameter:	12 in
Hub:	150 mm
Impeller Blades:	5
Pitch:	10 degrees
Blade Material:	Aluminium
Speed:	3500 RPM
Absorbed Power:	0.34 hp
Peak Power:	0.36 hp
Total Efficiency:	56 %

Motor Data (at STP)

Motor Type:	
Electrical Supply:	
Motor Frame/Power:	
Current FLC/Start:	
Motor Speed:	

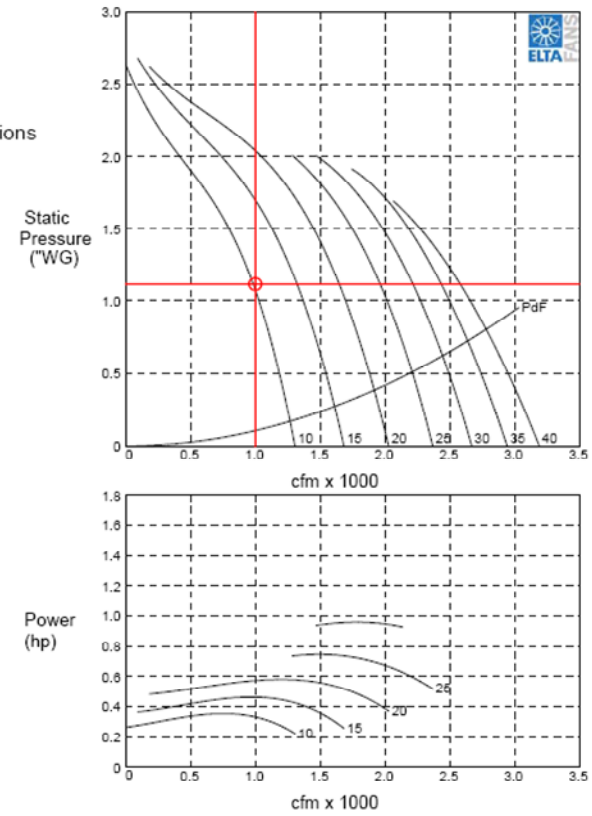

Sound Power

Density: 0.075 lbs/ft³

Spectrum (Hz)	63	125	250	500	1K	2K	4K	8K	dBW	dBA @ 5ft
Outlet PWL (dB)	83	84	84	80	79	78	75	68	90	70
Inlet PWL (dB)	81	82	83	78	76	78	72	64	89	69

Note: Levels are quoted as in-duct values. dBA values are average spherical free-field for comparitive use only.

Figure A3. ELTA fan data for model 012/150/5/10

Sample calculation of required RPM, to produce a desired pressure difference:

Fan Law Equations (Known: 20° blade angle, 3500 RPM, 1055 ACFM, 2.0 inH_2O)

$CFM2 = CFM1 \times (RPM2 / RPM1)$

$\Delta P_2 = \Delta P_1 \times (RPM_2 / RPM_1)^2$

$Power_2 = Power_1 \times (RPM_2 / RPM_1)^3$

Sea Level Example: 20° blade angle, *X* RPM, 1055 ACFM, **1.31 inH_2O**

$1.31 = 2.0 \times (RPM_2/3500)^2$

$RPM_2 = 2{,}832$

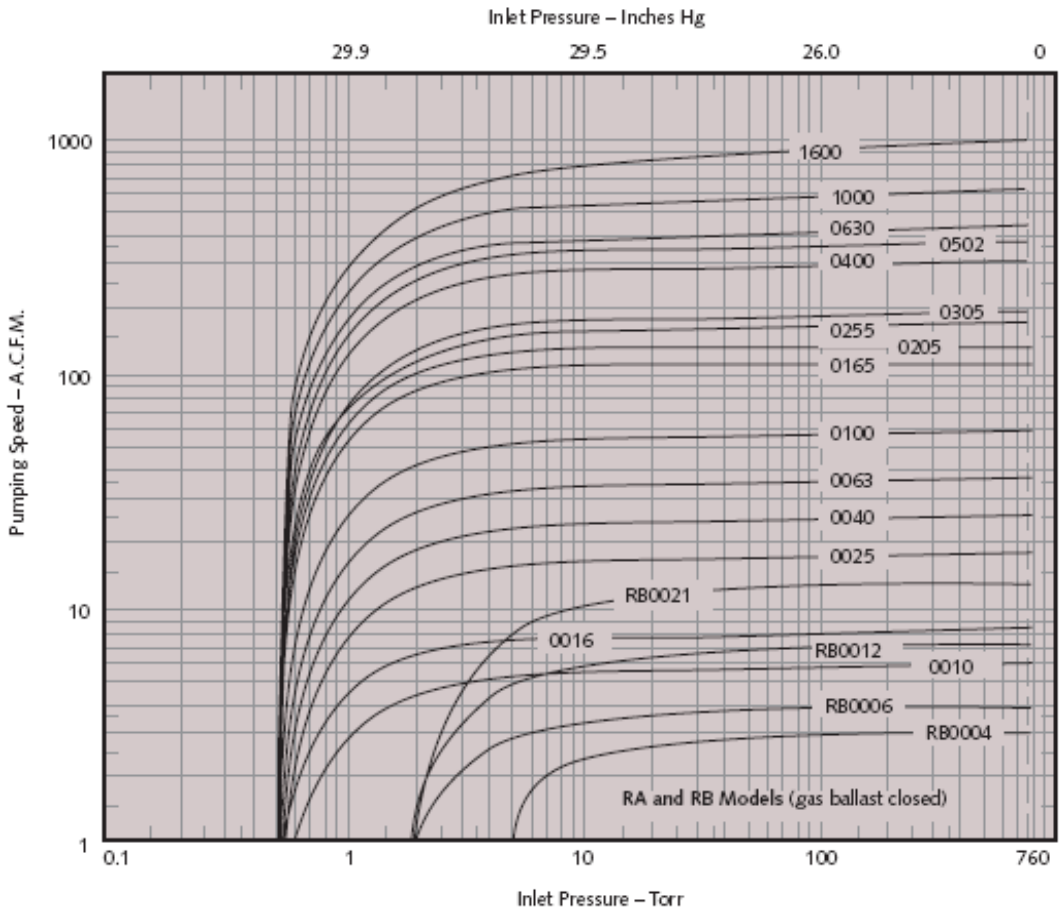

Figure A4. Vacuum pump performance curves for RA and RB models.

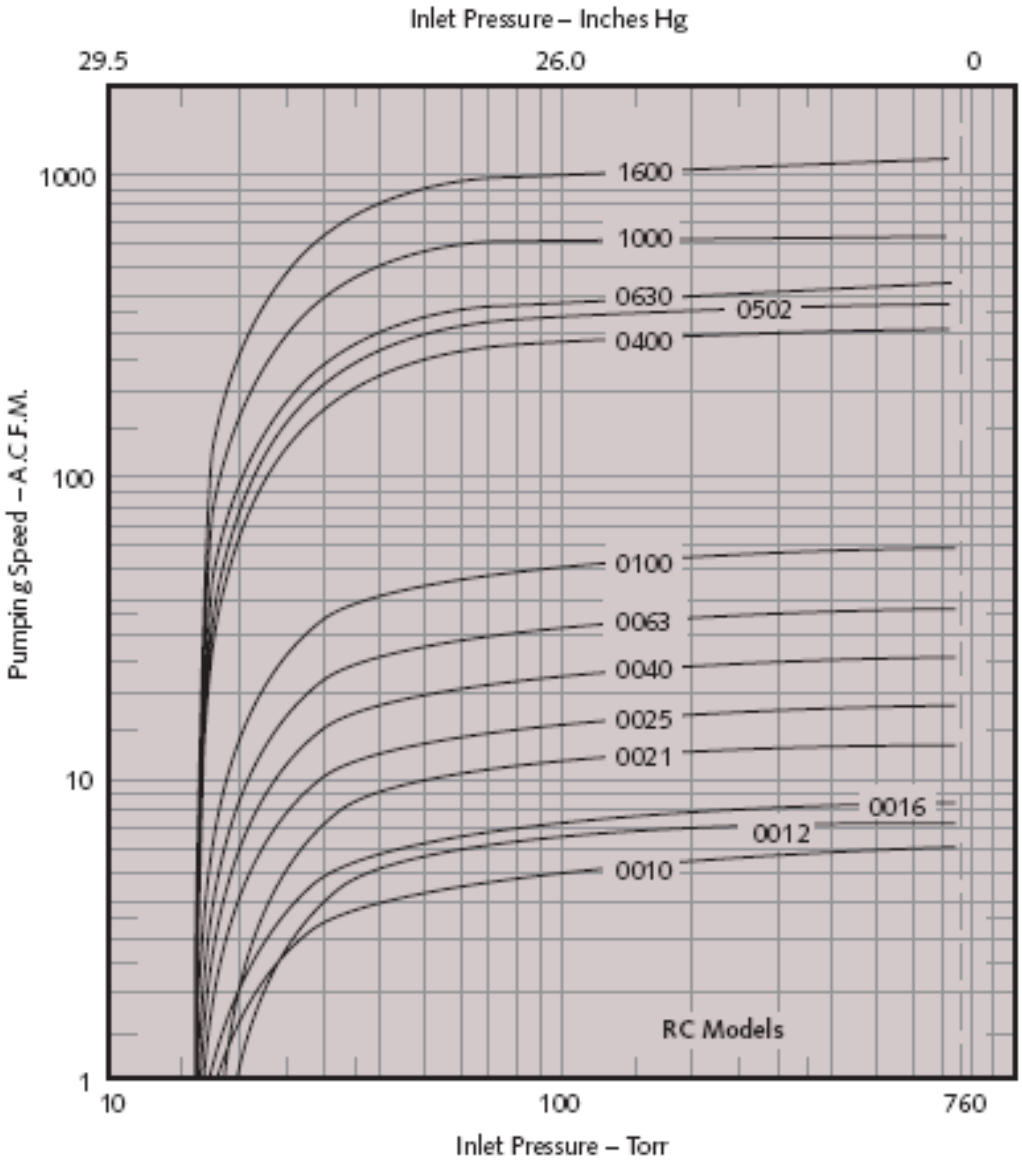

Figure A5. Vacuum pump performance curves for RC models.

APPENDIX B: IONIC ANEMOMETER DATA COLLECTION ERROR ASSESSMENT

B1. Introduction

The identification and measurement of clear air turbulence in the higher levels of the atmosphere (~ 60 000 ft) is of prime importance for the USAF. One instrument that shows great promise to measure turbulence data (time dependent velocity information) is the Ionic Anemometer.

The ionic anemometer is a unique instrument that uses a high voltage source to promote ion movement between charged rods (emitter and collector). The movement of these ions in air is sensitive to background wind velocity, air density and humidity levels. Activation voltage (the minimum voltage required to initiate ion motion) is strongly a function of air density. Lowering the air density also lowers activation voltage. A complete theory of the anemometer operation will not be provided here, but is available in the literature[1,2,3].

The ionic anemometer has existed at the research level for several decades but has never been developed into a commercial product. Therefore, attempts to deploy of this type of instrument typically require local manufacture (based upon design criteria outlined in the available literature). Very limited data exists for this type of instrument at high altitude (low density) conditions. As this instrument showed great promise, VSBYA fabricated an ionic anemometer in 2006. This device was tested at sea level flowing air conditions by VSBYA (see additional reports in this TR). Instrument response under these conditions was excellent. The instrument was next placed in a vacuum Bell jar to simulate response at high altitudes. The Bell jar test was able to establish an activation voltage vs. pressure curve for the instrument. The test results confirmed that activation voltage decreased significantly with decreasing air density. While in the Bell jar under vacuum, some tests of the instrument's ability to measure air velocity were conducted using a small fan. Though the arrangement did not allow for a quantitative evaluation, the results did prove that instrument response to changes in air velocity was quite good.

VSBYA was provided an opportunity to conduct high altitude turbulence data collection on the High Altitude Airship (HAA). To this end, a better understanding of the instruments response to velocity data at high altitude was needed to better quantify the instrument's suitability.

In 2006, visiting intern Mark Duell constructed a closed loop wind tunnel consisting of runs of 12" PVC piping and a section of 8" PVC piping in the actual test section. The air movement was provided by a 12" fan with a variable speed drive. Tunnel pressure was set by an externally controlled 30 SCFM vacuum pump that could vary vacuum level. Complete details are available in the body of this technical report . Data were collected by VSBYA Captain Barbeau at a density altitude corresponding to 138 millibars @ 15 ^{o}C and also at sea level, the results of which are reported in the main body of this Technical Report.

This document is provided as a means to estimate uncertainty associated data collected while using the VSBYA wind tunnel

B2. Uncertainty Overview

Ultimately, when collecting and post processing data the question that arises is "how accurate is the result"? A typical approach to answer this question is to conduct an uncertainty analysis. Several standards are available to conduct such an analysis. One such top level

standard is *International Organization for Standardization (ISO) "Guide to the Expression of Uncertainty in Measurement"*. This standard was published in 1993 and establishes general rules for evaluating and expressing uncertainty in measurements. One other standard often used in industry is *AMSE PTC 19.1-1998 "Test Uncertainty"*. Though the ASME standard closely follows the ISO standard, it is often preferred due to its more simplistic formulations and descriptions.

Detailed uncertainty theory will not be covered in this document. The reader is directed to the above standards for further information.

In general, uncertainty is an assessment of the errors associated with a given measurement (or product of measurements). Errors in measurement arise from several sources such as calibration errors, instrumentation placement errors, data acquisition hardware/software interface calibration or explicit errors, data collection methods and improperly collected transient information.

These errors are typically divided into two general categories:

1) Systematic Error (α) (often referred to as Bias error) is a portion of the total error that will essentially remain constant for repeated measurements of a parameter. One example of a systematic error would be an instrument calibration error.
2) Random Error (β) (often referred to as Precision error) is a portion of the total error that produces slight variation for repeated measurements of a parameter. These variations will show a distribution of data for a collected sample. Given enough samples, statistical methods can be used to determine an assumed true value of the measurement. The most common distribution of random error is the Gaussian or normal distribution. Successive readings will cluster about a central value and will extend over a limited interval surrounding the central value. For a Gaussian distribution, the average value of random error is zero. Quite often a Gaussian distribution is assumed when evaluating random error; however, for this assumption to be used, a minimum number of samples (usually 30 data samples or better) and/or other criteria may be required depending on type and methods of data collection.

Total error (uncertainty) combines all effects of Systematic and Random error. One common way to calculate uncertainty is through the method of *propagation of errors*. This method involves establishing *sensitivity factors.* Sensitivity is defined as the response of the final result to a slight variation in one of the measured parameters. Sensitivity factors can be calculated numerically, analytically, or in some cases measured directly from experimental data. For an example; if our end result G, relied on (or was a function of) measurements of parameters x, y, and z; then the sensitivities to parameters x, y, and z would be as follows:

$$\text{Assume } G(x,y,z) = (5x)(3y)/(z)$$

$$\text{Sensitivity of x on G} = \Delta G/\Delta x \text{ (at small } \Delta x) \text{ or } \frac{\partial G}{\partial x} = \frac{15y}{z}$$

Sensitivity of y on G = $\Delta G/\Delta y$ (at small Δy) or $\frac{\partial G}{\partial y} = \frac{15x}{z}$

Sensitivity of z on G = $\Delta G/\Delta z$ (at small Δz) or $\frac{\partial G}{\partial z} = -\frac{15xy}{z^2}$

As one might expect, measured parameters that produce the largest sensitivities produce the largest uncertainties in the end result.

Combining the effects of uncertainty is not just a simple matter of addition (see previous referenced standards). For a sufficient number of samples (> ~30) the following procedure is often employed to indicate 95% confidence:

Uncertainty of an individual measured parameter "x":

$$U_x = 2\sqrt{\alpha_x^{\,2} + \beta_x^{\,2}}$$

Where α (systematic error) and β (random error) are known (or estimated) based upon calibration information and statistical sampling.

Uncertainty of a calculated result (of more than one measured parameter):

$$U_{total} = \sqrt{\left(U_x \frac{\partial G}{\partial x}\right)^2 + \left(U_y \frac{\partial G}{\partial y}\right)^2 + \left(U_z \frac{\partial G}{\partial z}\right)^2 + \ldots} \text{ or } \sqrt{\sum \left(U_i \frac{\partial G}{\partial i}\right)^2}$$

The reporting of a calculated value (end result) will include the calculated value, the uncertainty and the confidence level used to obtain the uncertainty level. For example the measured value of heat load to air (Btu/hr) may have uncertainty expressed as a direct value or as a percentage value:

Heat Load "Q" = $Q_{measured}$ (Btu/hr) +/- 110 Btu/hr (95%)

or

Heat Load "Q" = $Q_{measured}$ (Btu/hr) +/- 4.5% (95%)

B3. Governing Equations and Measured Parameters for the Ionic Anemometer

The ionic anemometer is being employed to measure velocity. The value of *velocity* is to be inferred from voltage and current measurements to and from the instrument. Corrections must also be applied due to changes in density, applied voltage and humidity. Ultimately mean velocity and mean ionic anemometer current levels are evaluated to obtain the proportionality constant K, which will complete the equation:

$$v = K(I_2-I_1)/(I_2+I_1) + B$$

where v is velocity. Note that K and B will have units of velocity. B will be an experimentally determined zero offset. I_1 and I_2 are upwind and downwind collector currents respectively.

The VSBYA Ionic Anemometer used for the wind tunnel evaluation consisted of a specialized current sensing package developed by VSB electrical engineer Kris Robinson. This sensing package reported $(I_2-I_1) = \Delta$ and $(I_2+I_1) = \Sigma$, directly, in lieu of I_1 and I_2 individually. This was done in an effort to increase accuracy of the end result and aid in flexibility of data collection. This device also allowed for pre-zeroing of output data (in a known zero velocity flow), hence removing our offset constant B from the equation.

Our new equation becomes:

$$v = K\frac{\Delta}{\Sigma}$$

In general our overall assessment will be the result of tunnel inputs from:

- Instrument Input Voltage (V)
- Instrument Collector Current Difference (Δ)
- Instrument Collector Current Sum (Σ)
- Tunnel Absolute Pressure (P)
- Tunnel Fan Speed (ω), used to directly indicate tunnel wind *Velocity*
- Tunnel Temperature (T)

Additional errors in final result from:

- Placement of pressure taps
- Unknown tunnel turbulence levels
- Assumptions of accuracy with fan law equations in a low density environment
- Single point data sampling
- Un-calibrated pressure instruments
- Unknown tunnel humidity levels
- Tunnel Air Leaks
- Imprecise tunnel pressure control
- Non-exact instrument orientation in tunnel (ionic anemometer)
- Unknown tunnel velocity profile

We also know that Δ and Σ are affected by ion mobility. Ion mobility is strongly influenced by density, humidity and applied voltage. Therefore, all variables must be taken into account in the uncertainty analysis.

Governing equation(s):

$$K = \frac{v}{(\Delta)/(\Sigma)}$$

Where:

K = Proportionality Constant

v = Mean tunnel wind speed --> F(ω only)

Δ = Average Collector Current Difference --> F(P, T, Voltage(V) and Humidity(H))

Σ = Average Collector Current Sum --> F(P, T, V, and H)

The above implies that K = K(V, P, T, Δ, Σ, ω, H)

Overall uncertainty will take the form:

$$U_{total} = \sqrt{\left(U_V \frac{\partial K}{\partial V}\right)^2 + \left(U_P \frac{\partial K}{\partial P}\right)^2 + \left(U_T \frac{\partial K}{\partial T}\right)^2 + \left(U_\Delta \frac{\partial K}{\partial \Delta}\right)^2 + \left(U_\Sigma \frac{\partial K}{\partial \Sigma}\right)^2 + \left(U_\varpi \frac{\partial K}{\partial \varpi}\right)^2 + \left(U_H \frac{\partial K}{\partial H}\right)^2}$$

B4. Estimating the individual Ui's

Values for U_i's were computed utilizing OEM values for instrument accuracies and general estimates from the users (for α and β values). The following have been used as a basis for this evaluation:

Table B1: Uncertainty estimates for velocity measurements

	α Uncertainty				*β Uncertainty*		
	Value	***Units***	***Source***		***Value***	***Units***	***Source***
U_V α =	1.08	% Reading	Vendor Data	U_V β =	500	Volts	Estimate
U_P α =	5.0	millibar	Estimate	U_P β =	10.0	millibar	Estimate
U_T α =	0.5	°C	Estimate	U_T β =	2	°C	Estimate
U_Δ α =	1.05	% Reading	Vendor Data	U_Δ β =	0.03	μA	Estimate
U_Σ α =	1.05	% Reading	Vendor Data	U_Σ β =	0.05	μA	Estimate
U_ω α =	1.05	% Reading	Vendor Data	U_ω β =	1	Hz	Estimate
U_H α =	50	%	Estimate	U_H β =	50	%	Estimate

The ultimate values for $U_i = (\alpha_i^2 + \beta_i^2)^{0.5}$ will typically be unique for each data point when accuracy values are provided in *% of reading*, hence a Ui table is not provided here.

B5. Establishing Sensitivity Factors ($\partial K/\partial x_i$)

Evaluating our governing equation for all the variables listed above K(ω,Δ,Σ,V, P,T,H) is accomplished using a combination of analytical and empirical methods. The results are provided here, with details provided below.

Tunnel initial test calibration runs readily arrived at an expression for *Velocity* in terms of fan motor frequency ω. Though this probably could have been arrived at in an analytical fashion, the direct calibration of the tunnel against a precision turbine wind meter was a simple expedient and provided the following linear relationship. Note, a linear relationship was also expected due to incompressible fan theory and should also remain valid for lower density conditions).

Velocity (m/s) = 0.0206439(m/(s-Hz))*ω(Hz)

Our governing equation can now be written as:

$$K = \frac{0.0206439\,\varpi}{(\Delta)/(\Sigma)}$$

For the explicit variables ω, Δ and Σ, the needed partial derivatives can readily be evaluated as:

$$\frac{\partial K}{\partial \varpi} = 0.0206439 \, \Sigma / \Delta \qquad \text{(m/s(Hz))}$$

$$\frac{\partial K}{\partial \Delta} = -0.0206439 \, \varpi \, \Sigma / \Delta^2 \qquad \text{(m/(s-μA))}$$

$$\frac{\partial K}{\partial \Sigma} = -0.0206439 \, \varpi / \Delta \qquad \text{(m/(s-μA))}$$

Analytical expressions for dependence of K on V, P, T and H are not readily available. However, research from previous authors[1,2,3], and our test data can provide meaningful insight when estimating sensitivity factors for these variables. Small perturbations in actual test data for the variable in question (with all other variables held constant) can also provide a good estimate of the needed derivatives ($\frac{\partial K}{\partial x_i} \cong \frac{\Delta K}{\Delta x_i}$).

A review of J. Barat's paper *A High Resolution Anemometer for Boundary-Layer Measurements* reveals sensitivity assessments based upon measured response to parameter changes. Section 4 of his paper suggests the following:

<u>K sensitivity to Voltage Changes</u>:

$$K = K_0 \left[1 + 2.5E - 4\left(V - V_0\right) \right]$$

Where:

Ko = Constant corresponding to V=Vo
Vo = 5700Volts (for sea level conditions and his geometry)

This formulation was compared to our sea-level test data. Following Barat's methodology, an adjustment was made to the voltage constant yielding:

$$K = K_0 \left[1 + 3.8E - 4\left(V - V_0\right) \right]$$

As we were unable to collect good voltage perturbation data at altitude, we will assume that this sea-level sensitivity holds at altitude. This sensitivity is provided as:

$$\frac{\partial K}{\partial V} = 3.8x10^{-4} K_0 \quad \text{(m/(s V))}$$

(Note: VSB K_0 value is 30.70 m/s at sea-level)

K sensitivity to changes in Pressure Changes:

Note: Barat calls this sensitivity to density, though he only varies pressure.

$$K = K_o^{'}\left(1 + 0.07\left(\frac{Po - P}{P}\right)\right)$$

Where:

K_0' = Constant corresponding to $P=P_0$

P_0 = 1013mb (for sea level conditions and his geometry)

This would suggest:

$$\frac{\partial K}{\partial P} = \frac{-K_0' 0.07 Po}{P^2} \text{ m/(s mbar)}$$

This formulation is predicated on V = Vo = constant. Unfortunately, VSB data collection did not provide a ready means to verify this formulation (I.e. data not collected for pressure perturbations with voltage held constant). VSB data did, however, provide pressure perturbations with voltage set at *activation* for each pressure. Though not ideal (due to the varying voltage) this sensitivity factor has been estimated using:

$$\frac{\partial K}{\partial P} \cong \left(\frac{\Delta K}{\Delta P}\right)_{V_{Activation}} = -7.385x10^{-5} \quad \text{(m/(s mbar))}$$

K sensitivity to temperature:

We know from literature that ion mobility is strongly a function of the density of the flowing medium. The literature does not address any difference in density caused by temperature changes or pressure changes. As we cannot measure density directly (it becomes a calculated value from a measured P&T), we can only assume that the sensitivity found for pressure will be related to the sensitivity for temperature owing to an appropriate equation of state. As we are dealing with air at ambient temperatures (~ 15 ^{o}C), the *Ideal Gas Law* has been imposed for this purpose (P = ρRT, where R is the MW adjusted gas constant for air). Utilizing:

$$\frac{\partial K}{\partial T} \cong \frac{\partial K}{\partial P}\frac{\partial P}{\partial \rho}\frac{\partial \rho}{\partial T}$$

The *Ideal Gas Law* provides:

$$\frac{\partial P}{\partial \rho} = RT$$

$$\frac{\partial \rho}{\partial T} = -\frac{P}{RT^2}$$

$$\frac{\partial K}{\partial T} = \frac{\partial K}{\partial P}(RT)\frac{-P}{RT^2} = \frac{\partial K}{\partial P}\frac{-P}{T}$$

For the conditions of our test, the value of $\partial K/\partial P$ is:

$$\frac{\partial K}{\partial T} \cong 7.835x10^{-5}\frac{P}{T} \quad \text{(m/(s K))}$$

K sensitivity to humidity changes:

It is well known that ion mobility is sensitive to humidity levels (mobility decreasing with increasing humidity levels). Barat has provided the following based upon his collected test data at sea level.

$$K = K_0''(1 - 0.035H)$$

Where:

K_0'' = Constant corresponding to $H = 0.0$
H = Relative Humidity from 0.2 to 0.7

This would imply:

$$\frac{\partial K}{\partial H} = -K_0''(0.035) \quad \text{(m/s)}$$

for 50% humidity. For our use, we will use $K_0'' = 92.71$ m/s (our measured K at the 138 millibar test conditions).

Note: The above is formulated on Relative Humidity at sea-level. As relative humidity changes with pressure and temperature (for a given amount of moisture), it may make more sense to formulate in terms of Specific Humidity.

B6. Overall Uncertainty of a Test Point

The above uncertainties and sensitivities can now provide an estimate of the overall uncertainty of our proportionality constant K for each data point. This value can then be translated to an uncertainty in a calculated velocity by using the relations:

$$Velocity = \left(\frac{\Delta}{\Sigma}\right)\left(K \pm U_K\right) \quad \text{or} \quad U_{Velocity} = \left(\frac{\Delta}{\Sigma}\right)\left(\pm U_K\right)$$

B7. Results at the 138 mbar test condition

The above formulations have been utilized with our low pressure test data at 138 millibars. The plot below provides the uncertainty estimates as error bars on the plot.

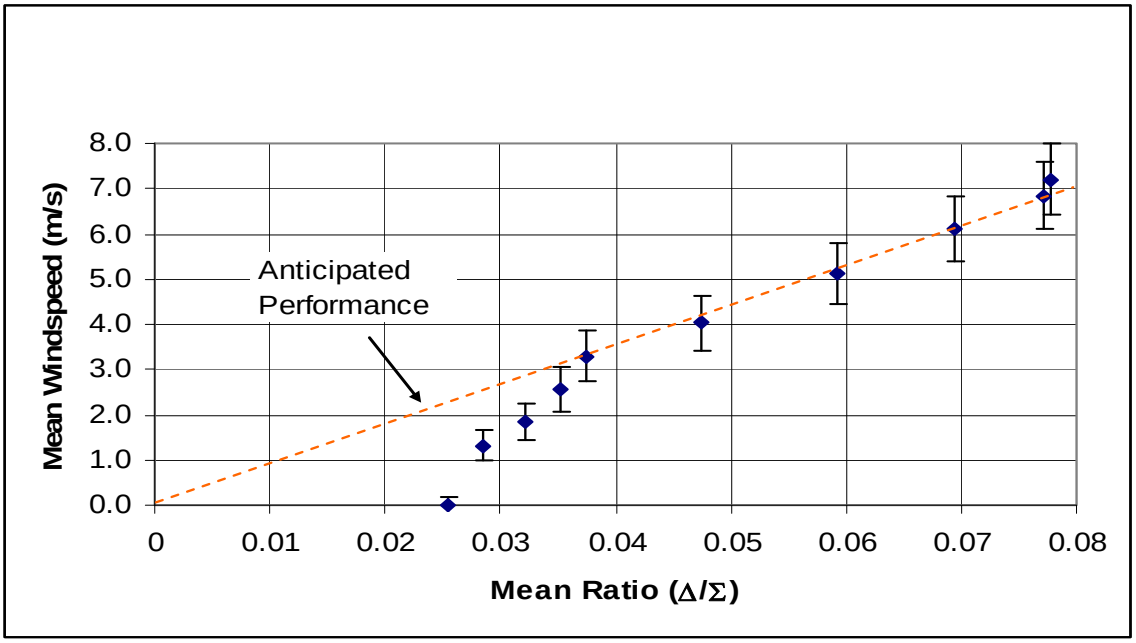

Figure B1. Conversion curve of mean windspeed vs. the mean ratio of the difference of current to the sum of the currents with estimated error bars on the data. Also shown is the anticipated behavior of the curve based on published performance of the ionic anemometer.

The plot provides a dotted line corresponding to the K value used for the sensitivity factors for this data set. From previous work, it is fully anticipated that the instrument's velocity response should be linear with respect to ratio (down to and including the zero velocity point). The indicated deviation below a ratio of 0.0375 will require further review to give us a better

understand the errors associated with these particular data points (as they fall well outside our estimated uncertainty bands). Data and corresponding uncertainties provided for ratio values greater than 0.0375 should remain valid however.

The above uncertainty review addresses steady state mean values for collected data only, and does not address uncertainties involved when using the instrument for turbulence data collection. It is assumed that the uncertainty associated with the mean values can also be applied to the turbulence; however this was not verified.

References

1. *A High-Resolution Ionic Anemometer for Boundary-Layer Measurements*, J. Barat, Journal of Applied Meteorology, V21, October 1982.
2. *An Ionization Anemometer,* J. Lovelock, *Journal of Scientific Instruments*, V26 November 1949.
3. *Modifications to the Omnidirectional Ionization Anemometer*, W. Welman, *Journal of Scientific Instruments*, V32, 1955.

NOMENCLATURE

a = Lift curve slope or a constant
b = Number of blades
c = Chord (m)
C_L = Coefficient of Lift (n.d.)
C_U^2 = Structure Constant for velocity $(m^{-2/3})/s^2$
D = Drag (N) or Diameter (m)
$D_{UU}(r)$ = Structure Function for velocity over a distance r (m^2/s^2)
E = Electric field (V/m)
Gr = Grashof Number (n.d.) (defined in Eq. 27)
g = Acceleration of gravity (m/s^2)
i = Ion current (A)
J = Moment of inertia (kg m^2)
K = Thermal conductivity (J/m K)
L = Lift (N)
M = Moment on the propeller shaft (Nm)
Nu = Nusselt Number (n.d.)
Pr = Prandtl Number (n.d.)
P, p = Pressure (Pa or millibars = hPa)
R = Radius of propeller blades (m)
r = Radius or distance (m)
s = Distance along a path (m)
T = Torque from propeller (Nm)
U, V = Velocity (m/s)
v = Velocity (mean or perturbation) (m/s)
Z = Height (m)
α = Angle of attack (deg) or thermal diffusivity (m^2/s)
Δ = Difference of the two ionic collector currents (A)
θ = Pitch angle of propeller blade (deg)
μ^+ = Mobility of ions (m^2/sV)
ν = Kinematic viscosity (m^2/s)
ρ = Density of the air (kg/m^3)
Σ = Sum of the two ionic collector currents (A)
Φ = Twist angle (deg)
Ω = Shaft angular velocity (rad/s)

Subscripts:

b = Velocity entering blade element
i = Index for two ionic velocity terms
M = Motor
o = Reduced mobility
P = Propeller
p = Velocity entering front of propeller anemometer
S = Shaft
$1,2$ = Collector elements of ionic anemometer, or locations along a streamline
∞ = Background flow (velocity)